LA-UR-17-22202 (Accepted Manuscript)

Quantification of water content by laser induced breakdown spectroscopy on Mars

Rapin, W.; Meslin, P.-Y.; Maurice, S.; Wiens, Roger Craig; Laporte, D.; Chauvire, B.; Gasnault, O.; Schroder, S.; Beck, P.; Bender, Steven Charles; Beyssac, O.; Cousin, A.; Dehouck, E.; Drouet, C.; Forni, O.; Nachon, M.; Melikechi, N.; Rondeau, B.; Thomas, N. H.

To be published in: Spectrochimica Acta Part B: Atomic Spectroscopy

DOI to publisher's version: 10.1016/j.sab.2017.02.007

Permalink to record: http://permalink.lanl.gov/object/view?what=info:lanl-repo/lareport/LA-UR-17-22202

Quantification of water content by laser induced breakdown spectroscopy on Mars

W. Rapin, P.-Y. Meslin, S. Maurice, R.C. Wiens, D. Laporte, B. Chauviré, O. Gasnault, S. Schröder, P. Beck, S. Bender, O. Beyssac, A. Cousin, E. Dehouck, C. Drouet, O. Forni, M. Nachon, N. Melikechi, B. Rondeau, N. Mangold, N.H. Thomas

PII: S0584-8547(17)30076-9
DOI: doi: 10.1016/j.sab.2017.02.007
Reference: SAB 5204

To appear in: *Spectrochimica Acta Part B: Atomic Spectroscopy*

Received date: 3 August 2016
Revised date: 2 February 2017
Accepted date: 10 February 2017

Please cite this article as: W. Rapin, P.-Y. Meslin, S. Maurice, R.C. Wiens, D. Laporte, B. Chauviré, O. Gasnault, S. Schröder, P. Beck, S. Bender, O. Beyssac, A. Cousin, E. Dehouck, C. Drouet, O. Forni, M. Nachon, N. Melikechi, B. Rondeau, N. Mangold, N.H. Thomas , Quantification of water content by laser induced breakdown spectroscopy on Mars. The address for the corresponding author was captured as affiliation for all authors. Please check if appropriate. Sab(2017), doi: 10.1016/j.sab.2017.02.007

Title:

Quantification of water content by laser induced breakdown spectroscopy on Mars

Authors:

W. Rapin[1,2], P.-Y. Meslin[1,2], S. Maurice[1,2], R. C. Wiens[3], D. Laporte[4], B. Chauviré[5], O. Gasnault[1,2], S. Schröder[1,2], P. Beck[6], S. Bender[3], O. Beyssac[7], A. Cousin[1,2], E. Dehouck[2], C. Drouet[8], O. Forni[1,2], M. Nachon[5], N. Melikechi[9], B. Rondeau[5], N. Mangold[5], N. H. Thomas[10]

Affiliations:

1 Université de Toulouse, UPS-OMP, Toulouse, France

2 Institut de Recherche en Astrophysique et Planétologie, CNRS, UMR 5277, Toulouse, France

3 Los Alamos National Laboratory, Los Alamos, New Mexico, USA

4 Laboratoire Magmas et Volcans, Université Blaise Pascal – CNRS – IRD, OPGC, Clermont-Ferrand, France

5 Laboratoire de Planétologie et Géodynamique, CNRS-UMR 6112, Nantes, France

7 Sorbonne Universités – CNRS UMR 7590, Institut de Minéralogie,

8 CIRIMAT Carnot Institute, UMR CNRS/INPT/UPS 5085, Université de Toulouse, ENSIACET, Toulouse, France

9 Optical Science Center for Applied Research, Delaware State University, Dover, DE, USA

10 California Institute of Technology, Division of Geological and Planetary Sciences, Pasadena, CA, United States

Highlights:

- Hydrated samples were analyzed using laser induced breakdown spectroscopy
- Experimental parameters were varied to test different types of signal normalization
- We obtain a calibration of the H signal applicable to a large range of martian data

Keywords: Laser-induced breakdown spectroscopy; ChemCam; hydrogen; water; hydration

Abstract:

Laser induced breakdown spectroscopy (LIBS), as performed by the ChemCam instrument, provides a new technique to measure hydrogen at the surface of Mars. Using a laboratory replica of the LIBS instrument onboard the Curiosity rover, different types of hydrated samples (basalts, calcium and magnesium sulfates, opals and apatites) covering a range of targets observed on Mars have been characterized and analyzed. A number of factors related to laser parameters, atmospheric conditions and differences in targets properties can affect the standoff LIBS signal, and in particular the hydrogen emission peak. Dedicated laboratory tests were run to identify a normalization of the hydrogen signal which could best compensate for these effects and enable the application of the laboratory calibration to Mars data. We check that the hydrogen signal increases linearly with water content; and normalization of the hydrogen emission peak using to oxygen and carbon emission peaks (related to the breakdown of atmospheric carbon dioxide) constitutes a robust approach. Moreover, the calibration curve obtained is relatively independent of the samples types.

I. Introduction

Hydrated phases are key markers of past climates in the geological record. The abundance of structural water within minerals can be a tracer of the specific conditions under which they formed, and underwent possible diagenesis. The water content of igneous rocks can also place important constraints on the type of magmatic activity and the geophysical evolution of the planet [1]. On Mars, hydrated minerals have been identified both from orbit [2–4] and in situ [5–7]. The estimation of water content at the surface of Mars, under low latitudes, has been limited to regional scale hydrogen maps [8–10], orbital infrared reflectance spectroscopy of water absorption bands but hindered by grain size and albedo effects [11–13], sparse and bulk pyrolysis experiments [14–16] and laboratory analyses of martian meteorites [17–20].

With the landing of the Curiosity rover on Mars at Gale crater, new means to characterize the surface hydration in situ have been deployed. The Dynamic Neutron Albedo (DAN) instrument, using a technique similar to orbital neutron detectors, passively or actively probes in situ the signature of hydrogen over a meter-scale surface and decimeters in

the subsurface [21]. The ChemCam instrument, located on the rover mast, performs stand-off laser induced breakdown spectroscopy (LIBS), a new technique to measure hydrogen at the surface of Mars [22,23]. The corresponding submillimeter measurements, an unprecedented analysis scale, have covered a large number of targets since landing (more than 10000 points on 1400 targets, ~350000 laser shots, up to the 1380th mission day, or sol, i.e. after over 2 Mars years). By providing elemental abundances, it is complementary to analyses performed by the CheMin (Chemistry and Mineralogy) instrument, which identifies hydrated minerals (among other crystalline phases) within drill samples by X-ray diffraction [7,24]. In particular, it was used to identify the hydrated nature of the amorphous phases found in the soils early in the mission [25]. The LIBS ability to measure elemental composition at a small scale, enabled finer scale geochemical analyses [26,27] and subsequent geological interpretations (e.g., [28–31]) although in these studies the hydrogen signal could not be used quantitatively.

The quantification of hydrogen by the measurement of the Balmer alpha emission peak (656.6 nm) is challenging because of the number of parameters which influence the LIBS signal. Stark broadening of the emission line is particularly important on hydrogen [32] and the peak is much wider at ambient terrestrial pressure than at low pressures. On Mars, the surface pressure of ~7 mbar is nearly optimal for the LIBS signal intensity [33] and the hydrogen peak is easily detected in the ChemCam data [34]. With regard to quantification, chemical and physical matrix effects have been proposed as an important source of uncertainty [34,35]. On the other hand, laboratory experiments at low pressures have shown a linear relationship between hydrogen signal intensity and water or hydrogen mass fraction [36,37].

The objective of this work is to perform extensive laboratory tests to study the ability to measure water content using the LIBS hydrogen Balmer alpha peak at 656.6 nm. First, the experimental setup, the acquisition and signal processing, and the choice of samples selected for this study are described, as well as the experimental parameters that were varied to account for the variability of conditions met on Mars and in the laboratory. Second, we summarize the results and discuss the effect of the different signal normalizations on the calibration process. Finally, the results are compared with independent measurements of water content performed on Mars, and we test possible applications of the method on martian LIBS data.

II. Materials and methods

ChemCam is the LIBS instrument suite located on the Curiosity rover remote sensing mast [22,23]. The laser beam at 1067 nm delivers 14 mJ on target with a pulse duration of 5 ns. A spectrometer collection time of 3 ms is used with no additional time gating; therefore, the entire plasma emission is recorded. The spectrometer covers the atomic emission peaks of interest within three different spectral ranges: 240-342 nm (ultra-violet, UV), 382-469 nm (blue-violet) and 474-906 nm (visible and near infrared, VNIR). The hydrogen Balmer alpha is the only hydrogen emission peak detectable by ChemCam, as other peaks from the Balmer series lie outside of the spectrometers range. Usual observations with the instrument consist of laser bursts, typically 30 shots at 3 Hz, on a given point; observations are repeated at closely spaced locations on the target. A spectrum is acquired for each laser pulse; and individual spectra can be averaged to improve signal to noise ratio on a single observation point. The first 5 shots can be ignored to remove the contribution from possible surface material (dust or thin coating). Additionally, the ChemCam remote micro imager (RMI) is used to document the target texture and precisely locate the sampling pits. The distance to the targets varies between 2.2 and 7 m, with most targets being at around 3 m.

Laboratory LIBS setup

The ChemCam Mast Unit Engineering Qualification model (MU EQM) combined with the body unit engineering model (BU EM) is the replica used in the laboratory at Institut de Recherche en Astrophysique et Planétologie (IRAP, Toulouse, France) for calibration purposes. The MU EQM is operated in a climate chamber at -10°C through a window similar to the Remote Warm Electronic Box (RWEB) setup on Mars. The instrument laser beam and line of sight is directed vertically onto a sample tray placed in a vacuum chamber using an adjustable mirror (fig. 1). It can be filled with a martian gas simulant (1.6 % argon, 2.7 % nitrogen and remaining carbon dioxide) to produce laser plasmas in conditions similar to Mars (hereafter called martian chamber). The typical distance to the targets in the laboratory is 1.6 m, similar to the distance to the calibration targets on the rover. Due to the additional optics (folding mirror and martian chamber entrance window), and differences in laser performance, the energy on target achieved in the laboratory (~10 mJ) is lower than usually used on Mars (~14 mJ). Tests described below have been performed to estimate the effect of laser energy on the LIBS hydrogen signal.

Laboratory samples

Several types of hydrated samples were analyzed in the laboratory (table 1). These were used to test chemical and physical matrix effects on the LIBS hydrogen signal and include a range of hydrated phases already identified by Curiosity on Mars. Ten basalt standards with water contents ranging from 0.18 to 2.2 wt % were synthesized at 1 GPa using a piston-cylinder apparatus housed at the "Laboratoire Magmas et Volcans" (in Clermont-Ferrand, France). The starting material was a powder of a fresh, non-altered basalt from the 2014 eruption of Bárðarbunga, Iceland (sample FL-3 [38]). The initial water content of the basaltic powder ($0.12 \pm 0.02[1\text{-}\sigma]$ wt %) was measured a dynamic flash combustion method (Thermo Scientific™ FLASH 2000 CHNS elemental analyzer). A technical requirement was that the basaltic standards were not translucent to avoid a weak laser coupling with target during LIBS analyses. Two different solutions were used to reach this goal. In the first series, the experiments were run below the liquidus temperature of the basalt so that the final products contained a large fraction of crystals in addition to glass. In this series, the run temperature ranged from 1200 °C (no added water) to 1130°C (2 wt % added H_2O) in order to keep the crystalline fraction nearly constant (between ~30 and 50 %). In the second experimental series, the run temperature was set to 1300°C, above the liquidus temperature, but the basalt powder was first oxidized in air at 800°C for 20 hours so that the final product was a dark brown glass with iron predominantly as Fe^{3+}. The basaltic standards (5 oxidized glasses and 5 partially crystallized basalts) can be used to test potential effects related to opacity and crystal size on the LIBS hydrogen signal.

Apart from the temperature and the degree of oxidation of the starting powder, the experimental techniques were the same in the two series: about 90 mg of basalt powder were loaded into a 4-mm diameter gold-palladium capsule along with 0 to 1.77 mg deionized water. The capsule was then welded shut and stored for 12 to 20 hours in an oven at 200°C to ensure a homogeneous distribution of water. The capsule was placed in a solid-media pressure assembly and subjected to a pressure of 1 GPa and a temperature of 1130 to 1300°C for two hours (see [39] for technical details on the piston-cylinder apparatus and the experimental assemblies). At the end of the experiments, the capsules were cut in three slices: the top and bottom slices were set aside for H analysis with the FLASH 2000 analyzer, and the intermediate slice (about 2 mm thick) was reserved for LIBS measurements. Additional

FTIR analyses were performed on the five oxidized glasses to have an independent estimate of their water content.

Pellets of synthetic hydroxyapatite, $Ca_{10}(PO_4)_6(OH)_2$, and fluorhydroxyapatite, $Ca_{10}(PO_4)_6F(OH)$, as well as intimate mechanical mixtures of these apatites with basalt (sample 2709SKA from Skjaldbreiður, Iceland), represent a total of 10 samples with a maximum water content equivalent of 1.7 wt.%. The two starting apatite powders were produced at the CIRIMAT laboratory (Toulouse, France). Hydroxyapatite was prepared by neutralization of phosphoric acid by dropwise addition of ammonia in the presence of calcium nitrate at boiling temperature, under constant stirring, and starting from stoichiometric Ca/P molar ratio. Partial fluorination to obtain the fluorhydroxyapatite phase, $Ca_{10}(PO_4)_6F(OH)$, was performed by heat treatment under argon gas flow (1 atm), using a tubular furnace with an alumina tube (internal diameter 4 cm), at 900°C for 1 hour and in the presence of NH_4F salt placed at the entrance of the tube. The apatite powders, pure or mixed with increasing proportions of basalt, were then pelletized (13-mm diameter) in a uniaxial press using a mechanical strain of 8 tons, and heated in air at 900°C for 1 hour, to remove any traces of excess water and for consolidation purposes. The presence and purity of the apatite minerals was verified by Raman spectroscopy and X-ray diffraction. The water content in the mixtures were estimated assuming stoichiometric hydroxyapatite and fluorhydroxyapatite compositions as listed above.

A large series of natural opals were analyzed [40]. While being mostly pure and therefore identical from a chemical standpoint, this collection of poorly crystalline silica phases shows diverse optical characteristics --translucent, opaque, fractured or smooth surface-- which are interesting to test with LIBS. The water content was estimated using loss on ignition (LOI) in air at 1000°C for ~20 hours. Additional thermogravimetric analysis (TGA) were used to check water loss measurements. Pellets of magnesium sulfate heptahydrate (epsomite) and hexahydrite were also tested, as well as calcium sulfates and mixtures with basalt powder (2709SKA) [41]. The water content was estimated using TGA at 200°C for calcium sulfates and LOI at 500°C for magnesium sulfates. Table 1 summarizes the sample series and methods used to characterize their water content. Although the samples contain H_2O or OH, the equivalent H_2O content -as a proxy for hydrogen content- will be used to represent calibration results.

Experimental LIBS methods

The samples were placed in the chamber pumped below 0.01 mbar within a few minutes. Depending on the behavior of the hydrous samples under vacuum, different protocols were used before introducing the martian gas simulant at ~8 mbar. The chamber with basalt standards, apatite pellets and apatite-basalt mixtures was pumped for at least 24 hours under primary vacuum to ensure removal of adsorbed water. Sulfates are delicate samples, which may lose water molecules under vacuum at ambient temperatures. Gypsum ($CaSO_4 \times 2H_2O$) was proven unstable at low H_2O partial pressures : Vaniman et al. [42] have shown that gypsum dehydration took ~50 hours to initiate at 24°C and a partial pressure of water in air of 0.007 mbar. A consistent result was observed in our laboratory: no weight loss observed for a gypsum pellet weighed before and after 20 hours under vacuum. Therefore, the gypsum pellets and gypsum-basalt mixtures were pumped for ~24 hours before LIBS analyses to remove adsorbed water from the basalt powder and preserve the gypsum structure. The pellets of bassanite ($CaSO_4 \times 0.5H_2O$), magnesium sulfate hexahydrite ($MgSO_4 \times 6H_2O$) and epsomite ($MgSO_4 \times 7H_2O$) proved to be unstable when exposed to vacuum for several hours. After 24 hours under vacuum the bassanite and epsomite pellets lost respectively ~50% and ~30% of their water content. Therefore, a shorter protocol was preferred for these samples: the chamber was pumped down to a pressure of 0.01 mbar within a few minutes, and the martian gas simulant was introduced at a pressure of ~8 mbar immediately after. During the subsequent LIBS analyses, the pressure was recorded to check sample degassing, but did not rise by more than 0.1 mbar. This is an important verification due to the sensitivity of LIBS hydrogen signal to the atmospheric water vapor pressure, which was investigated in a separate experiment described below.

The opal samples exhibited diverse behaviors when exposed to vacuum: some samples exchanged most adsorbed water within minutes and others were more stable. A different protocol was chosen to improve the estimate of water content during the LIBS tests for opals. The samples were exposed to vacuum for 24 hours prior to LIBS, then carefully weighed using a microgram-scale. The weight measured after LOI in air was compared to this weight obtained after exposure to vacuum to estimate water content during the LIBS tests.

Signal processing

Processing of the hydrogen signal is designed to extract the area of the hydrogen emission peak. It is located at 656.46 nm near a carbon peak doublet (C II 658.0 nm and C II 658.5 nm) forming a single peak in ChemCam spectra due to the instrument resolution of ~0.61 nm in that range. Due to the spectral proximity of hydrogen and carbon emission, the peaks are fitted simultaneously. A multi-Lorentz fitting method with a linear baseline curve fitting procedure similar to that reported by [34] and [41], was used. The hydrogen peak full width at half maximum (FWHM) is set to vary within bounds to best fit the observed data. Additional iron peaks (Fe I 654.8 nm and Fe I 659.4 nm) have been identified and observed for high iron targets, and are added to the fit for iron-bearing targets. Titanium emission peaks are also present (see Ti plate example in fig. 2) and the presence of other weak emission peaks is not excluded, but have not been clearly identified. Titanium is not included in the fits because this peak is expected to be negligible given the Ti abundances on Mars (the 'Ti plate' spectrum shown in Fig. 2 was obtained on the nearly pure Ti plate calibration target), and similarly the other unidentified contributions are supposed to be negligible in the fit. Figure 2 shows examples of the resulting fits.

For each LIBS point location, a spectrum without laser pulses is acquired in order to remove the background light from the target in the active spectra. As shown by Schröder et al. [34], this "dark removal" is particularly important to study the hydrogen signal because of the presence of the solar Balmer H absorption line observed in the background spectrum of targets illuminated by sunlight. While this is of importance for the martian spectra, laboratory spectra are not affected by such spectral features in the ambient lighting.

Hydrogen signal normalization

A number of experimental parameters affect the standoff LIBS signal. They are related to laser irradiance (laser energy, focus and distance to target), atmosphere (total pressure/density and composition) and target properties (different chemical/physical matrices and mixtures). Unlike well-constrained laboratory LIBS experiments, ChemCam is a survey instrument used under diverse conditions.

On Mars, variations due to target properties and differences in laser irradiance cannot be measured (or not precisely enough), or the effect on the signal is not easily predicted; consequently, we normalize the signals in order to compensate as much as possible for the undesired effects of these parameters. A number of relevant proxies are tested here for

normalization because they also reflect these variations: total spectrum intensity, continuum intensity or carbon or oxygen emission peaks from the breakdown of the martian atmospheric carbon dioxide. By normalization, we simply mean dividing by the value of the chosen normalizing proxy. As illustrated in figure 2, the area of the oxygen triplet (O I 777.5, 777.6 and 777.8 nm), forming a single peak in ChemCam spectra, is easily estimated. The carbon emission peak at 247.9 nm is estimated using a multi-Lorentz fit with a nearby iron peak (Fe I 248.3 nm) to subtract its contribution (figure 2). It is the only neutral carbon peak in ChemCam spectra. The normalization to carbon ionized emission peak (C II) at 658 nm is also tested. Its area is evaluated along with hydrogen as a result of the multi-Lorentz peak fitting (figure 2). The continuum intensity used for normalization is defined as the mean spectrum intensity in a peak-free wavelength range (similar to [34]). The interval chosen is from 680 to 690 nm where only minor interferences have been observed. The total spectrum intensity consists of the sum of spectral peaks (continuum removed) and is proposed either as the sum over the VNIR spectral range only, or the sum of all spectral ranges (UV, blue-violet and VNIR). To compute the total intensity of the spectral peaks only, a continuum removal processing is applied following a procedure similar to that described in [43]. We excluded normalization to specific sample elemental lines due to its intrinsic inability to correct for mixtures most often encountered in mineral assemblages found on natural rock targets. The ability of normalization proxies to compensate for the parameter variations has to be tested experimentally. The success criteria for the normalization proxies used here are the following: for targets with homogeneous hydrogen content, the normalized signal should be constant when experimental parameters (e.g., distance, laser energy density) are varied, and should minimize the standard deviation of the derived H abundance.

Homogeneous hydrated targets analyzed by ChemCam to support these tests exist on Mars. Calibration targets of known compositions have been mounted on the rover at a distance of 1.6 m from the instrument [44,45]. Most of these targets are depleted in water; only the macusanite, a natural obsidian, contains measurable H_2O (~0.5 wt.%) [46] but produces a low signal due to a weak laser-target coupling, as the sample is translucent. Other targets on Mars have shown interesting characteristics. First, the ubiquitous dust cover present on all undisturbed targets systematically affects the first shot of each laser burst. The resulting spectra reflect homogeneous chemistry, and a rather strong hydration signature [25,47]. Secondly, fracture-filling light-toned veins have been identified along the rover traverse as calcium sulfates without significant impurities [29]. This rather pure phase has a

defined chemical composition, which enables us to investigate hydration with negligible variation in chemical matrix. Thirdly, the rover drill was used to sample the bedrock at different locations. The collected material has been analyzed by two separate instruments performing X-Ray Diffraction (XRD) and Evolved Gas Analysis (EGA), both sensitive to hydrated phases. The ChemCam instrument targeted the drill hole wall at each location, analyzing newly exposed material. Providing sufficient homogeneity, these measurements are directly comparable with the drill sample.

Using both Mars data and laboratory measurements, each parameter affecting the LIBS signal was tested. The two criteria proposed above to determine which normalization of the hydrogen signal is best suited will be presented separately. The next section describes the tests conducted to check the variations implied by various parameters with results discussed in section 3, and the evolution of the standard deviation relative to mean for a given set of parameters is reported in table 2. The parameters, corresponding range and methods are detailed in the following paragraphs.

Dedicated LIBS parameters tests

ChemCam acquires LIBS spectra at distances between the laser and the target that vary between 2 and 7 m. Thus, a direct comparison of the LIBS spectra acquired at two or more distances is not trivial. [48,49] have shown that using a proxy spectroscopic standard created from first-shot dust observations on Mars targets minimizes the difference in spectral intensity measured at two different distances and increases spectral reproducibility. In this work, we use a similar approach that consists of evaluating the distance bias using dust sampled on Mars by the first laser shots. The hydrogen peak fit of the first shots is averaged within distance bins of 0.2 m from 2.2 to 4.8 m. There are at least 100 spectra in each bin (448 on average) so that the average result for each bin statistically minimizes the influence of other parameters related to laser focus or coupling with dust. Because the laser energy on target used in the laboratory is slightly different than that used on Mars, this parameter has been tested as well. On Mars, a subset of targets at short distances have been acquired using a lower laser energy. The first shots on dust for these targets are used to evaluate the effect of laser energy. The hydrogen signal from the first shots was averaged for a specific distance bin between 2.2 and 2.4 m for a total of 476 spectra at ~10 mJ on target and 673 spectra at ~14

mJ. Figure 3 represents the first shot hydrogen LIBS data separated into the two different laser energies and with varying distance.

The quality of the focus (which influences both laser irradiance and light collection) could be an important source of uncertainty on the standoff LIBS measurements, and therefore influence the hydrogen signal. The effect of laser focus was tested in the laboratory by sampling a homogeneous bassanite pellet at different points using different focuses. The focus is achieved by varying the position of the telescope's secondary mirror using a stepper motor. Maurice et al. [22] indicate that the irradiance decreases by 50% at ~ +/-20 motor steps from the best focus position on the Mars instrument. A similar variation of irradiance is expected in the laboratory as the telescope optics used are exact replicas. Laboratory tests were performed with some margin, as the position was varied by +/- 34 motor steps around the best focus position.

Variations in ambient pressure occur on Mars over a day and seasonally. Also, both pressure and density are known to affect the LIBS signal [33] and because of temperature, density is about 1.7 to 1.2 times greater on Mars than in the laboratory for the same pressure. Pressure was therefore varied from 7 to 17 mbar to cover the density variations encountered at Gale crater.

An additional experiment was conducted to test the effect of water vapor on the LIBS signal. Indeed, part of the hydrogen signal observed could come from the breakdown of atmospheric water molecules. Measurements on Mars might be affected by the presence of water vapor found in the atmosphere (although only at a 10-80 ppm level [50] [*Savijärvi et al.*, 2016a]), but more importantly, sample degassing can occur in the laboratory chamber under vacuum or at low pressures. It is therefore necessary to test the effect of the partial pressure of water vapor on the hydrogen signal to evaluate the influence of an atmospheric contribution. A water injection system was added to the chamber in order to control the addition of water vapor (fig. 1). An aluminum plate was used for the tests because its specific surface area is expected to be low and therefore limit contribution from adsorbed water. The tests were done for dry atmospheric conditions (with ~6.3 mbar of CO_2) after long term exposition to primary vacuum, and then with partial pressures of water vapor ranging from 0.002 mbar to 2.95 mbar.

The remaining parameters affecting the hydrogen signal are target-related and evaluated by testing various sample chemistries and aspects relevant to targets analyzed on

Mars. For each hydrogen signal normalization type, the standard deviation indicates how it is affected by the corresponding parameter variations (table 2).

Instrument response function correction

To compare the normalized hydrogen signal obtained in the laboratory with the data acquired on Mars, the difference in instrument response must be accounted for. Because the signal is normalized, only the relative instrument response function (IRF) is necessary to compare the normalized signals, i.e., the IRF ratio between the hydrogen signal spectral region at ~656 nm and the spectral area used for normalization. The instrument transmission ratio of the hydrogen region to the oxygen peak region at ~778 nm and to the carbon peak region at ~248 nm are significantly different between the laboratory replica and the flight instrument. It is mostly due to the use of additional optics in the laboratory and to different transmission functions of the BU EM and MU EQM compared to the flight model. The IRF has been measured on the flight model and spares prior to flight, but no end-to-end IRF was measured for the full setup in the laboratory. Therefore, normalization to total spectrum cannot be fully corrected for IRF, which prevents direct comparison to Mars using that particular norm. In the VNIR range, the IRF has been evaluated, accounting for additional optics transmission, and used to compute relative IRF between 656 nm and 778 nm. Another technique was used to estimate the relative IRF between the UV at 248 nm and the VNIR range. Figure 4 shows carbon at 248 nm and oxygen peak area at 778 nm obtained on pure or almost pure calcium sulfates both in the laboratory and on Mars (data listed in [41]). The signal varies by a factor of 5 to 10 for both instruments due to varying conditions. This is mostly due to variations in distance-to-target, laser focus quality, and laser-target coupling on Mars, and in the laboratory data was taken at set distance with varying laser focus and ambient pressure; see table 2. Yet, the two emission peaks area strongly correlate independently of the laser parameters and pressures used. Therefore, the change in regression slope between the two setups is attributable to the difference in relative IRF and is used to estimate the correction between 248 nm and 778 nm, and then the relative IRF between 778 nm and 656 nm is applied to be comparable to the hydrogen at 656 nm.

III. Results

The results obtained when varying each parameter separately (laser energy, focus, distance and pressure) are summarized in table 2 as point-to-point standard deviation. As an overall outcome, the tested normalizations generally reduce variations of the hydrogen signal. Table 2 shows that normalization to total spectrum, VNIR spectrum, neutral carbon at 248 nm, and oxygen lines, seem to produce more robust results than normalization to continuum or carbon at 658 nm. While the table summarizes data as standard deviation, we discuss here the variations with the parameters through minimum to maximum or signal increase *vs.* decrease. Using the first shots on dust and varying the distance from 2.2 to 4 m, the hydrogen signal decreases by 75% but only changes within 2.2%, 8% and 11% when normalized to oxygen, neutral carbon at 248 nm, and continuum, respectively (fig. 3). The effect of laser energy is also reduced by the different normalizations. Whereas the hydrogen signal decreases by 30% when the energy changes from ~14 mJ to ~10 mJ, it only changes within 1% and 4% of the average when normalized to neutral carbon and oxygen, respectively. However, normalization by the carbon ion peak at 658 nm does not produce the same result. Indeed, with the energy change from ~14 mJ to ~10 mJ, the intensity of this peak decreases by ~46%, while hydrogen only decreases by 30%, therefore the signal normalized to this peak increases for decreasing laser energy. The hydrogen signal normalized to carbon at 658 nm also increases with distance (fig. 3D). This suggests that the carbon peak at 658 nm is biased differently with laser irradiance than the other proxies. This behavior may be explained by the ionic nature of the doublet emission peak, whereas the carbon at ~248 nm and oxygen triplet at ~778 nm are neutral atomic emission peaks. The results in varying the laser focus show that the signal decreases by ~50% between best focus and out-of-focus limits. Normalization reduces these variations, significantly suppressing correlation with focus position (fig. 5).

Regarding the influence of pressure, the hydrogen signal area increases by 65% within the pressure range, but only increases by ~12% when normalized to carbon (248 nm) or oxygen (778 nm). However, normalization by the continuum does not help compensate for pressure because unlike hydrogen, the continuum intensity only increases by 9% over this low pressure range (fig. 6), resulting in a hydrogen signal increase of ~52% when normalized to continuum. This result shows that the atomic lines are more dependent on atmospheric pressure than the continuum emission, and could be used to correct part of this effect.

The result of the experiment with water vapor injection is shown in figure 7. The linear regression leads to a detection threshold of ~ 0.1 mbar. On Mars at Gale crater, the

partial pressure of water vapor remains below 0.0014 mbar [51], which is well below the estimated threshold. Additionally, there is no hydrogen signal observed on the hydrogen-free calibration targets (fig. 2) [34]. This confirms that the atmospheric water vapor contribution is negligible on Mars. However, degassing in the laboratory test chamber could easily generate 0.1 mbar water vapor during tests. Therefore, pressure was carefully monitored during calibration tests.

Laboratory calibration

The calibration curve obtained from the series of homogenous samples analyzed in the laboratory at ~1.6 m with varying types and water content is shown on figure 8. For each sample the LIBS data is the average of several points, taking for each point the mean spectrum of 30 shots with the first 5 shots removed. Figure 8-A shows the hydrogen peak area using no normalization. It may thus highlight the scatter resulting from varying laser coupling efficiencies among targets. The scatter could be also attributed to chemical matrix effects, reflecting the fact that a specific target chemistry affects the plasma emission, leading to different hydrogen emission intensities for similar hydrogen mass fraction. The scatter observed on the data from opals also highlights physical matrix effects. Indeed, the opals tested have the same chemical composition ($SiO_2.nH_2O$), so part of the scatter observed in the non-normalized hydrogen calibration data is probably due to different optical properties related to the samples. The fragments have been analyzed with different surface textures: sawed, polished, fresh fracture surface and also turned into fine-grained pellets. Figure 8-B to G show the calibration normalized using the different proxies for coupling. Most of these normalization techniques seem to reduce the data scatter, compared to using no norm. While the continuum normalization appears less robust to physical matrix effects as seen on the result for opals, and the normalization to total emission less robust to chemical matrix effects, normalization to neutral carbon peak or oxygen peak compensates best for both effects. The figures show a good linearity and highlight that the linearity is valid for a large range of sample physical and chemical matrices.

The uncertainty on water prediction associated with each linear calibration model can be estimated using the root mean square error (RMSE) of the linear regression. Accounting for all samples, the RMSE correspond to a precision of ±1.2 wt.% and ±1.7 wt.% water content when using the neutral carbon and oxygen norm, respectively. It is noteworthy that

this precision can be improved by limiting the calibration to specific sample types or to lower water content. The detection threshold of the measurement is difficult to evaluate due to the residual hydrogen peak still observed in the laboratory on presumably anhydrous samples (anhydrite and silicon wafer). The presence of the relatively intense nearby carbon peak at 658 nm implies difficulties in fitting low hydrogen signals. However, tests performed under vacuum show that a hydrogen signal is observed which confirms the presence of hydrogen in the target even at the lowest abundances. Figure 9 illustrates the hydrogen signal from the basalt glass containing 0.18 wt.% (as measured using the FLASH 2000 analyzer) along with the other nominally anhydrous samples. The signal observed is even lower in the latter, which suggests that the detection threshold should be on the order of 0.18 wt.% H_2O or lower. When using the calibration on Mars data normalized to carbon at 248 nm or oxygen at 778 nm, the difference in IRF and its associated uncertainty must also be taken into account. The corresponding uncertainty on the true value is given as a percentage of the predicted value, ~30% for normalization to oxygen at 778 nm and ~33% for carbon at 248 nm.

Effects of the sample surface

Variations of the signal within shot-to-shot profiles have been observed in the laboratory. Since the samples have been selected for their homogeneity, shot profile variation is a metrological issue related to the LIBS technique and needs to be addressed. Within each shot series, the hydrogen signal intensity observed in the first shot is usually higher than the average. This effect related to the sample surface has been reported in the literature [37] and mostly attributed to the presence of an ubiquitous surface layer of water molecules and hydroxyls. This contribution can be removed using a laser cleaning technique, where a series of laser shots are performed, slightly out of focus to increase the ablated spot size. Due to uncertainty of focusing using ChemCam on Mars, no precise offset position can be achieved to enhance laser cleaning at remote distances but one can simply remove the 5 first shots. To test such a surface effect, measurements were performed in the laboratory on a basalt standard containing 0.18 wt.% of bulk H_2O with and without performing laser cleaning. The sample was stored under vacuum for 20 hours, then observed with LIBS under 8.8 mbar of martian gas simulant. A first series of 4 points, 30 shots each, was performed on the exposed sample surface. Then a ~1 x 1 mm area was cleaned by sweeping 120 laser pulses across it. Then a single point measurement with 150 shots was performed at the center of the area. The pit size, ~300 µm, was fully within the cleaned surface area. Figure 10 shows the result

before and after the laser cleaning was applied. The hydrogen signal of the first shot after laser cleaning is lower than the first shots before, but still higher than the average. This suggests the method could not fully remove the surface hydrogen signal but was efficient at reducing it. It is likely that trace amounts of water vapor re-adsorbed on the surface after the cleaning and before the 150-shot analysis. More importantly, the result on the average hydrogen signal with 5 first shots removed was not affected. This confirms that using the five first shots for cleaning, as used for the calibration data and for processing of ChemCam LIBS data in general, is an efficient technique for removing most of the effects related to surficial, weakly-bounded water.

Shot profile variations

For specific samples, the LIBS signal varies gradually with shot number. In particular, for sulfate pellets and opals, the hydrogen signal decreases strongly with shot number while the continuum intensity increases, as seen on figure 11. In contrast, synthetic basaltic rock standards and apatite pellets do not show significant variations. Since the samples were chosen to be homogeneous with depth, the observed variation is probably either due to a plasma effect related to the change of crater geometry, and/or also possibly due to local dehydration induced by heating from the laser pulses. To investigate the possibility of dehydration, the pits were analyzed using Raman spectroscopy. The Raman data were obtained using a Renishaw INVIA microspectrometer operating at IMPMC. Spectra were measured directly on the raw samples at constant room temperature using the 514.5 nm wavelength of a 50 mW Modulaser (green laser). The sampling spot of ~1-2 µm allowed us to analyze within and out of the pit cavities (~300 µm diameter) and was used to test homogeneity. The laser power delivered at the sample surface was set to less than 5 mW to prevent irreversible thermal damage.

The gypsum pellet ($CaSO_4 \times 2H_2O$) showed no changes of the Raman signal in the range 100-2000 cm^{-1} where occur (i) the internal vibration modes of the SO_4 tetrahedra and (ii) the crystal lattice modes, between the LIBS cavity and the unaltered sample surface. This suggests that the laser shot did not affect the structural state of gypsum. In the range 3000-4000 cm^{-1} where occurs the stretching vibration modes of O-H in water, a subtle difference in the relative peak intensities is observed only locally in the LIBS cavity compared to the unaltered sample surface. This suggests that dehydration, if any, was only very light and local

in the LIBS cavity. On the bassanite pellet, the signature in the LIBS pit shows greater fluorescence hindering the Raman signal, maybe due to local structural disruption or amorphization. Opal samples have been tested as well but only display strong fluorescence hindering the Raman signal with no specific change inside the pits. Overall the fluorescence mostly hindered the Raman peak signal, so the results were inconclusive, except on gypsum for which the LIBS hydrogen signal decreases with shot number whereas no evidence for dehydration was found using Raman spectroscopy. Therefore, some of these variations could be attributed to a LIBS plasma effect. The empirical approach of finding a proxy to limit the variability and possible decrease of the hydrogen signal with depth in homogeneous samples was also applied.

Table 2 shows the standard deviation of the hydrogen signal for several profiles measured in the laboratory and for different normalizations. Normalization to carbon and oxygen tend to reduce the shot-to-shot variability. In contrast, normalization to the continuum emission increases the signal variation over the depth profile. Figure 11 highlights the fact that the continuum emission increases with shot number. This behavior was already documented in LIBS and was proven to correlate with the volume of the pit cavity [52]. This increase with pit depth may be attributed to plasma confinement within the cavity. The decrease of the hydrogen signal with depth has been documented as well [37] but the phenomena producing this effect have not been clearly identified yet. The normalization to carbon or oxygen is found to limit the variations but still exhibit a decrease for some samples as shown in figure 11. The opal samples have shown different behaviors with regard to shot profile variations. Depth profile experiments have been performed and they show that the hydrogen signal does not tend towards zero but stabilizes with increasing shot number. Figure 12 shows how the calibration curves could depend on the number of shots chosen. To summarize, the behavior observed on shot-to-shot profiles is sample-dependent despite the use of normalizations. A 30 shot protocol was chosen for this study because it is the protocol chosen for most ChemCam observations performed on Mars. The shot profile variability shall be investigated further in a separate study.

IV. Discussion

The results obtained from the tests presented here highlight the metrological issues associated with the quantitative measure of hydrogen using the LIBS by ChemCam, and help

estimate the value of each normalization. In the following discussion, we provide updated results on the data used for the study on calcium sulfates [41] and discuss the consistency of the result provided by all normalizations. Finally, the calibration results are compared to independent measurements of the water content by other instruments onboard Curiosity.

Evaluation of the different types of normalization

The differences implied by the choice of normalization can be summarized based on the experimental results described above. Overall, the calibration curve obtained under well-constrained conditions in the laboratory is found to increase monotonously, with a clearly reduced amount of scatter when using normalization to oxygen and neutral carbon emission lines. Normalization to continuum, however, does not correct for atmospheric pressure effect and amplifies variations within shot-to-shot profiles (table 2). The ionic carbon line is found to be less reliable to correct variations related to laser irradiance. The normalization to total intensity or VNIR spectrum intensity is not optimal and not well suited for application to Mars hydrogen data because the difference in IRF is not fully characterized yet for the particular setup used here. This norm is also intrinsically dependent on the number and intensity of peaks within the spectrometer ranges, which may vary among different sample chemical matrices. It may explain part of the scatter obtained in the calibration trend using this type of normalization. Of the emission lines investigated for this work, neutral carbon at 247 nm or the neutral oxygen triplet at 778 nm are the two best options for normalization. Although this aspect was not investigated here, the oxygen peak partly originates from sample oxides and could be biased by the sample bulk oxygen content. However, the variation of the oxygen content is small in most martian targets. On the other hand, the carbon peak at 248 nm may be difficult to fit accurately in the case of targets with high-iron content because of interferences with iron peaks, as illustrated in the examples on figure 2. Also, while most martian rocks are expected to be mostly carbon-free, this normalization could be biased when targeting carbonates or organic materials, if these were to be encountered.

To confirm that normalizations compensate for differences of laser parameters between the laboratory setup and Mars, targets accessible to both instruments could be used. The macusanite is the only water-bearing calibration target available both in the laboratory and on Mars [46], and may therefore be used for this validation. Although the laser-target coupling is low, producing a rather low signal with respect to other calibration targets, a

hydrogen signal is obtained on this target with both instruments. Figure 13 shows that despite instrument inequalities, the signal from the laboratory matches that from Mars when normalized to carbon at 248 nm or oxygen from the laboratory and Mars match in both cases. This validates the IRF correction and the ability of these norms to correct for the differences in laser irradiance.

Robustness of the result on calcium sulfates at Gale crater

Using data obtained on almost pure calcium sulfate veins on Mars and the same laboratory calibration method, we were able to show that most veins at Gale crater have a homogenous hydration signature consistent with that of bassanite [41]. The calibration of the water content made for that study used a normalization of the hydrogen signal to the neutral carbon peak (C I at 247.9 nm) and is very consistent with the calibration obtained here with an extended and more diverse set of samples. To test the robustness of the method, the same calibration of the martian data was performed using the different available norms. Figure 14 represents the reference signal obtained in the laboratory for gypsum (theoretical water content of 20.1 wt.%), bassanite (typical water content of 6.2 wt.%) and anhydrite compared to martian data. Correction for differences in IRF was applied for normalization to carbon and oxygen peaks. Using normalization to oxygen, carbon at 248 nm and at 658 nm, or total and VNIR spectrum intensity, the result is unambiguously consistent with the hydration level characteristic of bassanite. The normalization to the continuum produces a different result: it increases the scatter in the signal measured on martian veins, rising above the laboratory reference for bassanite and reaching that of gypsum. This behavior is specific to the continuum, whose intensity increases with shot number, as discussed above and illustrated in figure 11. The shot-to-shot profiles measured on calcium sulfate veins on Mars were averaged and are shown in figure 15. They are compared with shot-to-shot profiles obtained using laboratory pellets. In both cases, the continuum is seen to increase, although the increase is stronger in the laboratory (40% between shots 5-10 and 25-30) than on Mars (~9%). When normalized to the carbon peak at ~248 nm, the signal profile is more steady and consistent with bassanite (fig. 14-B). This result is consistent with XRD analyses of samples including veinlets which revealed the presence of bassanite but not gypsum [7], as discussed in a separate study [41].

Comparison to other instruments

Additionally, water abundances measured by other instruments onboard Curiosity can be compared with corresponding calibrated ChemCam data. In particular, mudstones at Gale crater have been sampled by the rover drill at several locations along the traverse. As mentioned previously, the ChemCam instrument sampled several points onto the drill hole wall at each site. The ChemCam data were checked for homogeneity and then averaged over all points on the drill hole wall. Figure 16-A shows the bulk water content of the drill samples measured by the SAM instrument using EGA [16] is similar to the average water content derived from the ChemCam hydrogen signal normalized to oxygen using the calibration work presented here (fig. 8). Moreover, the Dynamic Albedo of Neutron (DAN) instrument measures the abundance of water in the shallow subsurface by the neutron-absorbing signature of hydrogen [21]. The instrument has been used near the drilling sites, and the homogeneity of the sedimentary rocks sampled suggests the possibility to cross-compare the different instruments at these locations. However, heterogeneity with depth could be a source of uncertainty when comparing the result of a ~6 cm drill sample with integrations depth over tens of centimeters for the DAN active observations. Despite these limitations, Figure 16-B shows a good agreement of the water equivalent hydrogen measured by DAN and ChemCam.

V. Conclusion

This study highlights new results with regard to the quantification of hydrogen using the LIBS technique in general, and applicable to the ChemCam instrument data in particular. Several parameters affecting the standoff LIBS signal have been tested. The emission peaks related to atmospheric breakdown of CO_2 are shown to be good proxies to compensate for the signal variations over a large range of experimental conditions, enabling the use of most of the data acquired on Mars. A series of samples covering distinct chemical matrices and varying water contents were analyzed. The hydrogen signal, normalized using different proxies, increases linearly with water content up to ~50 wt.% for a large range of sample types. Normalization to neutral carbon or oxygen peaks both minimize the calibration curve statistical error but represent different tradeoffs depending on the context of use. The oxygen peak intensity is stronger than carbon and free of interference with other elemental lines, however part of the peak signal is related to the ubiquitous presence of oxygen in the samples encountered at Gale crater. Although not fully tested in this study, the varying amount of oxygen in the samples could be a source of uncertainty when using this norm for calibration. By contrast, the carbon peak emission originates almost entirely from the atmosphere due to

the absence or negligible amounts of carbon compounds in the martian regolith; however, nearby iron peaks interfere with the signal for high iron targets. In the case of calcium sulfate veins, we have shown that the detection of bassanite is robust to all the normalizations used, except with the continuum, which yields a larger dispersion of the water content. Variations within shot-to-shot profiles have been observed on Mars and in the laboratory. According to the Raman spectroscopy analysis performed at the laboratory, this could not be attributed to sample dehydration at least for gypsum and remains to be explained.

The Curiosity rover traverse at Gale crater includes various geological units with hydrated phases identified from orbit, including sulfates and clay minerals [53]. Based on the calibration results, the ChemCam instrument can be used to place constraints on the level of hydration for a large range of materials. Targets of specific interest with respect to hydration include igneous rocks, where the question of the water content of the magmas has major implications for crustal evolution [19]. The surface expression is expected to be in the form of apatites [54] or amphiboles, the presence of the latter still being speculative [55]. Sedimentary bedrock targets are of interest in terms of hydration as a way to understand their phyllosilicate contents. Concretions and diagenetic crystal forms observed on the surfaces of sedimentary rocks are also of interest, to understand their mineral structure and provenance [56,57]. A final example is high-silica bedrock and high-silica alteration halos [58]. Dedicated studies should help evaluate water content of these targets using the LIBS hydrogen signal for the first time on Mars, and explore the corresponding geological implications.

Acknowledgments:

This research was funded by Université Paul Sabatier as part of a PhD thesis [59], and LIBS experiments were conducted at Institut de Recherche en Astrophysique et Planétologie (IRAP) with support from CNES. Olgeir Sigmarsson and Claire Fonquernie from Laboratoire Magmas et Volcans are thanked for providing the basalt sample WM23 and for making the hydrogen analyses with the FLASH 2000 CHNS elemental analyzer, respectively. The authors thankfully recognize the help of Ludovic Cicutto, for the preparation of apatite samples and laboratory analyses, and Fleur Olagnier during LIBS tests with water vapor. The authors also thank one anonymous reviewer for his helpful comments.

References:

[1] B.O. Mysen, D. Virgo, R.K. Popp, C.M. Bertka, The role of H2O in Martian magmatic systems, Am. Mineral. 83 (1998) 942–946.

[2] J.-P. Bibring, Y. Langevin, J.F. Mustard, F. Poulet, R. Arvidson, A. Gendrin, G. Neukum, et al., Global Mineralogical and Aqueous Mars History Derived from OMEGA/Mars Express Data, Science. 312 (2006) 400–404. doi:10.1126/science.1122659.

[3] J.F. Mustard, S.L. Murchie, S.M. Pelkey, B.L. Ehlmann, R.E. Milliken, J.A. Grant, J.-P. Bibring, F. Poulet, J. Bishop, E.N. Dobrea, L. Roach, F. Seelos, R.E. Arvidson, S. Wiseman, R. Green, C. Hash, D. Humm, E. Malaret, J.A. McGovern, K. Seelos, T. Clancy, R. Clark, D.D. Marais, N. Izenberg, A. Knudson, Y. Langevin, T. Martin, P. McGuire, R. Morris, M. Robinson, T. Roush, M. Smith, G. Swayze, H. Taylor, T. Titus, M. Wolff, Hydrated silicate minerals on Mars observed by the Mars Reconnaissance Orbiter CRISM instrument, Nature. 454 (2008) 305–309. doi:10.1038/nature07097.

[4] J. Carter, F. Poulet, J.-P. Bibring, N. Mangold, S. Murchie, Hydrous minerals on Mars as seen by the CRISM and OMEGA imaging spectrometers: Updated global view, J. Geophys. Res. Planets. 118 (2013) 831–858. doi:10.1029/2012JE004145.

[5] J.L. Campbell, R. Gellert, M. Lee, C.L. Mallett, J.A. Maxwell, J.M. O'Meara, Quantitative in situ determination of hydration of bright high-sulfate Martian soils, J. Geophys. Res. Planets. 113 (2008) E06S11. doi:10.1029/2007JE002959.

[6] S.W. Squyres, R.E. Arvidson, S. Ruff, R. Gellert, R.V. Morris, D.W. Ming, L. Crumpler, J.D. Farmer, D.J.D. Marais, A. Yen, S.M. McLennan, W. Calvin, J.F. Bell, B.C. Clark, A. Wang, T.J. McCoy, M.E. Schmidt, P.A. de Souza, Detection of Silica-Rich Deposits on Mars, Science. 320 (2008) 1063–1067. doi:10.1126/science.1155429.

[7] D.T. Vaniman, D.L. Bish, D.W. Ming, T.F. Bristow, R.V. Morris, D.F. Blake, M.-P.Z. Mier, et al., Mineralogy of a Mudstone at Yellowknife Bay, Gale Crater, Mars, Science. 343 (2014) 1243480. doi:10.1126/science.1243480.

[8] W.C. Feldman, T.H. Prettyman, S. Maurice, J.J. Plaut, D.L. Bish, D.T. Vaniman, M.T. Mellon, A.E. Metzger, S.W. Squyres, S. Karunatillake, W.V. Boynton, R.C. Elphic, H.O. Funsten, D.J. Lawrence, R.L. Tokar, Global distribution of near-surface hydrogen on Mars, J. Geophys. Res. Planets. 109 (2004) E09006. doi:10.1029/2003JE002160.

[9] W. v. Boynton, G. j. Taylor, L. g. Evans, R. c. Reedy, R. Starr, D. m. Janes, K. e. Kerry, D. m. Drake, K. j. Kim, R. m. s. Williams, M. k. Crombie, J. m. Dohm, V. Baker, A. e. Metzger, S. Karunatillake, J. m. Keller, H. e. Newsom, J. r. Arnold, J. Bruckner, P. a. j. Englert, O. Gasnault, A. l. Sprague, I. Mitrofanov, S. w. Squyres, J. i. Trombka, L. d'Uston, H. Wanke, D. k. Hamara, Concentration of H, Si, CI, K, Fe, and Th in the low- and mid-latitude regions of Mars, J. Geophys. Res. - Part E - Planets. 112 (2007) (15 pp.). doi:10.1029/2007JE002887.

[10] S. Maurice, W. Feldman, B. Diez, O. Gasnault, D.J. Lawrence, A. Pathare, T. Prettyman, Mars Odyssey neutron data: 1. Data processing and models of water-equivalent-hydrogen distribution, J. Geophys. Res. Planets. 116 (2011) E11008. doi:10.1029/2011JE003810.

[11] D. Jouglet, F. Poulet, R. e. Milliken, J. f. Mustard, J.-P. Bibring, Y. Langevin, B. Gondet, C. Gomez, Hydration state of the Martian surface as seen by mars express OMEGA: 1. Analysis of the 3 μm hydration feature, J. Geophys. Res. - Part E - Planets. 112 (2007) (20 pp.). doi:10.1029/2006JE002846.

[12] R.E. Milliken, J.F. Mustard, F. Poulet, D. Jouglet, J.-P. Bibring, B. Gondet, Y. Langevin, Hydration state of the Martian surface as seen by Mars Express OMEGA: 2. H2O content of the surface, J. Geophys. Res. Planets. 112 (2007) E08S07. doi:10.1029/2006JE002853.

[13] J. Audouard, F. Poulet, M. Vincendon, R.E. Milliken, D. Jouglet, J.-P. Bibring, B. Gondet, Y. Langevin, Water in the Martian regolith from OMEGA/Mars Express, J. Geophys. Res. Planets. 119 (2014) 2014JE004649. doi:10.1002/2014JE004649.

[14] K. Biemann, J. Oro, P. Toulmin Iii, L.E. Orgel, A.O. Nier, D.M. Anderson, P.G. Simmonds, D. Flory, A.V. Diaz, D.R. Rushneck, J.A. Biller, Search for organic and volatile inorganic compounds in two surface samples from the Chryse Planitia region of Mars, Science. 194 (1976) 72–76.

[15] P.H. Smith, L.K. Tamppari, R.E. Arvidson, D. Bass, D. Blaney, W.V. Boynton, A. Carswell, D.C. Catling, B.C. Clark, T. Duck, E. DeJong, D. Fisher, W. Goetz, H.P. Gunnlaugsson, M.H. Hecht, V. Hipkin, J. Hoffman, S.F. Hviid, H.U. Keller, S.P. Kounaves, C.F. Lange, M.T. Lemmon, M.B. Madsen, W.J. Markiewicz, J. Marshall, C.P. McKay, M.T. Mellon, D.W. Ming, R.V. Morris, W.T. Pike, N. Renno, U. Staufer, C. Stoker, P. Taylor, J.A. Whiteway, A.P. Zent, H2O at the Phoenix Landing Site, Science. 325 (2009) 58–61. doi:10.1126/science.1172339.

[16] D.W. Ming, P.D. Archer, D.P. Glavin, J.L. Eigenbrode, H.B. Franz, B. Sutter, M.S. Team, et al., Volatile and Organic Compositions of Sedimentary Rocks in Yellowknife Bay, Gale Crater, Mars, Science. 343 (2014) 1245267. doi:10.1126/science.1245267.

[17] L.A. Leshin, S. Epstein, E.M. Stolper, Hydrogen isotope geochemistry of SNC meteorites, Geochim. Cosmochim. Acta. 60 (1996) 2635–2650. doi:10.1016/0016-7037(96)00122-6.

[18] J. Filiberto, A.H. Treiman, Martian magmas contained abundant chlorine, but little water, Geol. Boulder. 37 (2009) 1087–1090. doi:10.1130/G30488A.1.

[19] F.M. McCubbin, A. Smirnov, H. Nekvasil, J. Wang, E. Hauri, D.H. Lindsley, Hydrous magmatism on Mars: A source of water for the surface and subsurface during the Amazonian, Earth Planet. Sci. Lett. 292 (2010) 132–138. doi:10.1016/j.epsl.2010.01.028.

[20] C.B. Agee, N.V. Wilson, F.M. McCubbin, K. Ziegler, V.J. Polyak, Z.D. Sharp, Y. Asmerom, M.H. Nunn, R. Shaheen, M.H. Thiemens, A. Steele, M.L. Fogel, R. Bowden, M. Glamoclija, Z. Zhang, S.M. Elardo, Unique Meteorite from Early Amazonian Mars: Water-Rich Basaltic Breccia Northwest Africa 7034, Science. 339 (2013) 780–785. doi:10.1126/science.1228858.

[21] I. Mitrofanov, M. Litvak, A. Varenikov, Y. Barmakov, A. Behar, Y. Bobrovnitsky, E. Bogolubov, W. Boynton, K. Harshman, E. Kan, A. Kozyrev, R. Kuzmin, A. Malakhov, M. Mokrousov, S. Ponomareva, V. Ryzhkov, A. Sanin, G. Smirnov, V. Shvetsov, G. Timoshenko, Dynamic Albedo of Neutrons (DAN) Experiment Onboard NASA's Mars Science Laboratory, Space Sci. Rev. 170 (2012) 559–582. doi:10.1007/s11214-012-9924-y.

[22] S. Maurice, R.C. Wiens, M. Saccoccio, B. Barraclough, O. Gasnault, O. Forni, D. Vaniman, et al., The ChemCam Instrument Suite on the Mars Science Laboratory (MSL) Rover: Science Objectives and Mast Unit Description, Space Sci. Rev. 170 (2012) 95–166. doi:10.1007/s11214-012-9912-2.

[23] R.C. Wiens, S. Maurice, B. Barraclough, M. Saccoccio, W.C. Barkley, J.F.B. Iii, B. Wong-Swanson, et al., The ChemCam Instrument Suite on the Mars Science Laboratory (MSL) Rover: Body Unit and Combined System Tests, Space Sci. Rev. 170 (2012) 167–227. doi:10.1007/s11214-012-9902-4.

[24] D. Blake, D. Vaniman, C. Achilles, R. Anderson, D. Bish, T. Bristow, C. Chen, S. Chipera, J. Crisp, D. Des Marais, R.T. Downs, J. Farmer, S. Feldman, M. Fonda, M. Gailhanou, H. Ma, D.W. Ming, R.V. Morris, P. Sarrazin, E. Stolper, A. Treiman, A. Yen, Characterization and Calibration of the CheMin Mineralogical Instrument on Mars Science Laboratory, Space Sci. Rev. 170 (2012) 341–399. doi:10.1007/s11214-012-9905-1.

[25] P.-Y. Meslin, O. Gasnault, O. Forni, S. Schröder, A. Cousin, G. Berger, J. Berger, et al., Soil Diversity and Hydration as Observed by ChemCam at Gale Crater, Mars, Science. 341 (2013) 1238670. doi:10.1126/science.1238670.

[26] R.C. Wiens, S. Maurice, M.S. Team, ChemCam: Chemostratigraphy by the First Mars Microprobe, Elements. 11 (2015) 33–38. doi:10.2113/gselements.11.1.33.

[27] S. Maurice, S.M. Clegg, R.C. Wiens, O. Gasnault, W. Rapin, O. Forni, A. Cousin, V. Sautter, N. Mangold, L.L. Deit, M. Nachon, R.B. Anderson, N.L. Lanza, C. Fabre, V. Payré, J. Lasue, P.-Y. Meslin, R.J. Léveillé, B.L. Barraclough, P. Beck, S.C. Bender, G. Berger, J.C. Bridges, N.T. Bridges, G. Dromart, M.D. Dyar, R. Francis, J. Frydenvang, B. Gondet, B.L. Ehlmann, K.E. Herkenhoff, J.R. Johnson, Y. Langevin, M.B. Madsen, N. Melikechi, J.-L. Lacour, S.L. Mouélic, E. Lewin, H.E. Newsom, A.M. Ollila, P. Pinet, S. Schröder, J.-B. Sirven, R.L. Tokar, M.J. Toplis, C. d'Uston, D.T. Vaniman, A.R. Vasavada, ChemCam activities and discoveries during the nominal mission of the Mars Science Laboratory in Gale crater, Mars, J. Anal. At. Spectrom. 31 (2016) 863–889. doi:10.1039/C5JA00417A.

[28] R.J. Léveillé, J. Bridges, R.C. Wiens, N. Mangold, A. Cousin, N. Lanza, O. Forni, A. Ollila, J. Grotzinger, S. Clegg, K. Siebach, G. Berger, B. Clark, C. Fabre, R. Anderson, O. Gasnault, D. Blaney, L. Deflores, L. Leshin, S. Maurice, H. Newsom, Chemistry of fracture-filling raised

ridges in Yellowknife Bay, Gale Crater: Window into past aqueous activity and habitability on Mars, J. Geophys. Res. Planets. 119 (2014) 2014JE004620. doi:10.1002/2014JE004620.

[29] M. Nachon, S.M. Clegg, N. Mangold, S. Schröder, L.C. Kah, G. Dromart, A. Ollila, J.R. Johnson, D.Z. Oehler, J.C. Bridges, S. Le Mouélic, O. Forni, R. c. Wiens, R.B. Anderson, D.L. Blaney, J. f. Bell, B. Clark, A. Cousin, M.D. Dyar, B. Ehlmann, C. Fabre, O. Gasnault, J. Grotzinger, J. Lasue, E. Lewin, R. Léveillé, S. McLennan, S. Maurice, P.-Y. Meslin, W. Rapin, M. Rice, S.W. Squyres, K. Stack, D.Y. Sumner, D. Vaniman, D. Wellington, Calcium sulfate veins characterized by ChemCam/Curiosity at Gale crater, Mars, J. Geophys. Res. Planets. 119 (2014) 2013JE004588. doi:10.1002/2013JE004588.

[30] N. Mangold, O. Forni, G. Dromart, K. Stack, R.C. Wiens, O. Gasnault, D.Y. Sumner, M. Nachon, P.-Y. Meslin, R.B. Anderson, B. Barraclough, J.F. Bell, G. Berger, D.L. Blaney, J.C. Bridges, F. Calef, B. Clark, S.M. Clegg, A. Cousin, L. Edgar, K. Edgett, B. Ehlmann, C. Fabre, M. Fisk, J. Grotzinger, S. Gupta, K.E. Herkenhoff, J. Hurowitz, J.R. Johnson, L.C. Kah, N. Lanza, J. Lasue, S. Le Mouélic, R. Léveillé, E. Lewin, M. Malin, S. McLennan, S. Maurice, N. Melikechi, A. Mezzacappa, R. Milliken, H. Newsom, A. Ollila, S.K. Rowland, V. Sautter, M. Schmidt, S. Schröder, C. d'Uston, D. Vaniman, R. Williams, Chemical variations in Yellowknife Bay formation sedimentary rocks analyzed by ChemCam on board the Curiosity rover on Mars, J. Geophys. Res. Planets. 120 (2015) 2014JE004681. doi:10.1002/2014JE004681.

[31] V. Sautter, M.J. Toplis, R.C. Wiens, A. Cousin, C. Fabre, O. Gasnault, S. Maurice, O. Forni, J. Lasue, A. Ollila, J.C. Bridges, N. Mangold, S. Le Mouélic, M. Fisk, P.-Y. Meslin, P. Beck, P. Pinet, L. Le Deit, W. Rapin, E.M. Stolper, H. Newsom, D. Dyar, N. Lanza, D. Vaniman, S. Clegg, J.J. Wray, In situ evidence for continental crust on early Mars, Nat. Geosci. 8 (2015) 605–609. doi:10.1038/ngeo2474.

[32] L. Pardini, S. Legnaioli, G. Lorenzetti, V. Palleschi, R. Gaudiuso, A. De Giacomo, D.M. Diaz Pace, F. Anabitarte Garcia, G. de Holanda Cavalcanti, C. Parigger, On the determination of plasma electron number density from Stark broadened hydrogen Balmer series lines in Laser-Induced Breakdown Spectroscopy experiments, Spectrochim. Acta Part B At. Spectrosc. 88 (2013) 98–103. doi:10.1016/j.sab.2013.05.030.

[33] A.K. Knight, N.L. `rbarth, D.A. Cremers, M.J. Ferris, Characterization of laser-induced breakdown spectroscopy (LIBS) for application to space exploration, Appl. Spectrosc. (2000). doi:10.1366/0003702001949591.

[34] S. Schröder, P.-Y. Meslin, O. Gasnault, S. Maurice, A. Cousin, R.C. Wiens, W. Rapin, M.D. Dyar, N. Mangold, O. Forni, M. Nachon, S. Clegg, J.R. Johnson, J. Lasue, S. Le Mouélic, A. Ollila, P. Pinet, V. Sautter, D. Vaniman, Hydrogen detection with ChemCam at Gale crater, Icarus. 249 (2015) 43–61. doi:10.1016/j.icarus.2014.08.029.

[35] P. Sobron, A. Wang, F. Sobron, Extraction of compositional and hydration information of sulfates from laser-induced plasma spectra recorded under Mars atmospheric conditions — Implications for ChemCam investigations on Curiosity rover, Spectrochim. Acta Part B At. Spectrosc. 68 (2012) 1–16. doi:10.1016/j.sab.2012.01.002.

[36] J. Lasue, R.C. Wiens, S.M. Clegg, D.T. Vaniman, K.H. Joy, S. Humphries, A. Mezzacappa, N. Melikechi, R.E. McInroy, S. Bender, Remote laser-induced breakdown spectroscopy (LIBS) for lunar exploration, J. Geophys. Res. Planets. 117 (2012) E01002. doi:10.1029/2011JE003898.

[37] K.H. Kurniawan, M.O. Tjia, K. Kagawa, Review of Laser-Induced Plasma, Its Mechanism, and Application to Quantitative Analysis of Hydrogen and Deuterium, Appl. Spectrosc. Rev. 49 (2014) 323–434. doi:10.1080/05704928.2013.825267.

[38] O. Sigmarsson, S.A. Halldorsson, Delimiting Baroarbunga and Askja volcanic systems with Sr- and Nd-isotope ratios, Jokull. 65 (2015) 17–28.

[39] D. Laporte, M.J. Toplis, M. Seyler, J.-L. Devidal, A new experimental technique for extracting liquids from peridotite at very low degrees of melting: application to partial melting of depleted peridotite, Contrib. Mineral. Petrol. 146 (2003) 463–484. doi:10.1007/s00410-003-0509-3.

[40] B. Chauviré, B. Rondeau, N. Mangold, Near Infrared signature of opal and chalcedony as a proxy for their condition of formation, Am. Mineral. (submitted).

[41] W. Rapin, P.-Y. Meslin, S. Maurice, D. Vaniman, M. Nachon, N. Mangold, S. Schröder, O. Gasnault, O. Forni, R.C. Wiens, Hydration state of calcium sulfates in Gale crater, Mars: identification of bassanite veins, EPSL. (submitted).
[42] D.T. Vaniman, D.L. Bish, S.J. Chipera, Calcium Sulfate Hydration, Stability and Transformation on Mars, in: 2008: p. 1816.
[43] R.C. Wiens, S. Maurice, J. Lasue, O. Forni, R.B. Anderson, S. Clegg, S. Bender, D. Blaney, B.L. Barraclough, A. Cousin, L. Deflores, D. Delapp, M.D. Dyar, C. Fabre, O. Gasnault, N. Lanza, J. Mazoyer, N. Melikechi, P.-Y. Meslin, H. Newsom, A. Ollila, R. Perez, R.L. Tokar, D. Vaniman, Pre-flight calibration and initial data processing for the ChemCam laser-induced breakdown spectroscopy instrument on the Mars Science Laboratory rover, Spectrochim. Acta Part B At. Spectrosc. 82 (2013) 1–27. doi:10.1016/j.sab.2013.02.003.
[44] C. Fabre, S. Maurice, A. Cousin, R.C. Wiens, O. Forni, V. Sautter, D. Guillaume, Onboard calibration igneous targets for the Mars Science Laboratory Curiosity rover and the Chemistry Camera laser induced breakdown spectroscopy instrument, Spectrochim. Acta Part B At. Spectrosc. 66 (2011) 280–289. doi:10.1016/j.sab.2011.03.012.
[45] D. Vaniman, M.D. Dyar, R. Wiens, A. Ollila, N. Lanza, J. Lasue, J.M. Rhodes, S. Clegg, H. Newsom, Ceramic ChemCam Calibration Targets on Mars Science Laboratory, Space Sci. Rev. 170 (2012) 229–255. doi:10.1007/s11214-012-9886-0.
[46] C. Fabre, S. Maurice, A. Cousin, R.C. Wiens, O. Forni, V. Sautter, D. Guillaume, Onboard calibration igneous targets for the Mars Science Laboratory Curiosity rover and the Chemistry Camera laser induced breakdown spectroscopy instrument, Spectrochim. Acta Part B At. Spectrosc. 66 (2011) 280–289. doi:10.1016/j.sab.2011.03.012.
[47] J. Lasue, S. Maurice, A. Cousin, O. Forni, P.Y. Meslin, W. Rapin, S. Schroeder, A. Ollila, G. Berger, N. Bridges, S.M. Clegg, C. d'Uston, C. Fabre, O. Gasnault, W. Goetz, J. Johnson, N. Lanza, S. Le Mouélic, M.B. Madsen, N. Mangold, N. Melikechi, A. Mezzacappa, H. Newsom, R.C. Wiens, MSL Science Team, ChemCam Analysis of Martian Fine Dust, in: 2014: p. 1224. http://adsabs.harvard.edu/abs/2014LPI....45.1224L (accessed November 27, 2015).
[48] N. Melikechi, A. Mezzacappa, A. Cousin, N.L. Lanza, J. Lasue, S.M. Clegg, G. Berger, R.C. Wiens, S. Maurice, R.L. Tokar, S. Bender, O. Forni, E.A. Breves, M.D. Dyar, J. Frydenvang, D. Delapp, O. Gasnault, H. Newsom, A.M. Ollila, E. Lewin, B.C. Clark, B.L. Ehlmann, D. Blaney, C. Fabre, Correcting for variable laser-target distances of laser-induced breakdown spectroscopy measurements with ChemCam using emission lines of Martian dust spectra, Spectrochim. Acta Part B At. Spectrosc. 96 (2014) 51–60. doi:10.1016/j.sab.2014.04.004.
[49] A. Mezzacappa, N. Melikechi, A. Cousin, R. c. Wiens, J. Lasue, S. m. Clegg, R. Tokar, S. Bender, N. l. Lanza, S. Maurice, G. Berger, O. Forni, O. Gasnault, M. d. Dyar, T. Boucher, E. Lewin, C. Fabre, Application of distance correction to ChemCam laser-induced breakdown spectroscopy measurements, Spectrochim. Acta Part B At. Spectrosc. 120 (2016) 19–29. doi:10.1016/j.sab.2016.03.009.
[50] H. Savijärvi, A.-M. Harri, O. Kemppinen, The diurnal water cycle at Curiosity: Role of exchange with the regolith, Icarus. 265 (2016) 63–69. doi:10.1016/j.icarus.2015.10.008.
[51] H. Savijärvi, A.-M. Harri, O. Kemppinen, The diurnal water cycle at Curiosity: Role of exchange with the regolith, Icarus. 265 (2016) 63–69. doi:10.1016/j.icarus.2015.10.008.
[52] D. Devismes, B.A. Cohen, P.Y. Gillot, Developing a Relationship Between LIBS Ablation and Pit Volume for In Situ Dating of Geologic Samples, in: 2015: p. 1406. http://adsabs.harvard.edu/abs/2015LPI....46.1406D (accessed May 10, 2016).
[53] R.E. Milliken, J.P. Grotzinger, B.J. Thomson, Paleoclimate of Mars as captured by the stratigraphic record in Gale Crater, Geophys. Res. Lett. 37 (2010) @CitationL04201-@CitationL04201. doi:10.1029/2009GL041870.
[54] O. Forni, M. Gaft, M.J. Toplis, S.M. Clegg, S. Maurice, R.C. Wiens, N. Mangold, O. Gasnault, V. Sautter, S. Le Mouélic, P.-Y. Meslin, M. Nachon, R.E. McInroy, A.M. Ollila, A. Cousin, J.C. Bridges, N.L. Lanza, M.D. Dyar, First detection of fluorine on Mars: Implications for Gale Crater's geochemistry, Geophys. Res. Lett. 42 (2015) 2014GL062742. doi:10.1002/2014GL062742.
[55] A. Cousin, V. Sautter, V. Payré, O. Forni, Classification of Igneous Rocks analyzed by ChemCam at Gale Crater, Mars, Icarus. (submitted).

[56] L.C. Kah, M.S. Team, Images from Curiosity: A New Look at Mars, Elements. 11 (2015) 27–32. doi:10.2113/gselements.11.1.27.

[57] M. Nachon, N. Mangold, O. Forni, L.C. Kah, A. Cousin, R.C. Wiens, R. Anderson, D. Blaney, J.G. Blank, F. Calef, S.M. Clegg, C. Fabre, M.R. Fisk, O. Gasnault, J.P. Grotzinger, R. Kronyak, N.L. Lanza, J. Lasue, L.L. Deit, S.L. Mouélic, S. Maurice, P.-Y. Meslin, D.Z. Oehler, V. Payré, W. Rapin, S. Schröder, K. Stack, D. Sumner, Chemistry of diagenetic features analyzed by ChemCam at Pahrump Hills, Gale crater, Mars, Icarus. (2016). doi:10.1016/j.icarus.2016.08.026.

[58] J. Frydenvang, P.J. Gasda, J.A. Hurowitz, J.P. Grotzinger, R.C. Wiens, H.E. Newsom, J. Bridges, O. Gasnault, S. Maurice, M. Fisk, B. Ehlmann, J. Watkins, N. Stein, O. Forni, N. Mangold, A. Cousin, S.M. Clegg, R.B. Anderson, V. Payré, W. Rapin, D. Vaniman, R.V. Morris, D. Blake, S. Gupta, V. Sautter, P.-Y. Meslin, P. Edwards, M. Rice, K.M. Kinch, R. Milliken, R. Gellert, L. Thompson, B.C. Clark, K.S. Edgett, D. Sumner, A. Fraeman, M.B. Madsen, I. Mitrofanov, I. Jun, F. Calef, A.R. Vasavada, Discovery of Silica-Rich Lacustrine and Eolian Sedimentary Rocks in Gale Crater, Mars, in: 2016: p. 2349. http://adsabs.harvard.edu/abs/2016LPI....47.2349F (accessed May 24, 2016).

[59] W. Rapin, Hydratation de la surface de Mars à partir des données du rover Curiosity, Université de Toulouse, 2017.

[60] A. Cousin, V. Sautter, N. Mangold, C. Fabre, O. Forni, W. Rapin, M. Fisk, O. Gasnault, N. Lanza, J. Lasue, P.Y. Meslin, H. Newsom, A. Ollila, V. Payre, R.C. Wiens, S. Maurice, Igneous Rock Classification at Gale (Sols 13-800), in: 2015: p. 2452. http://adsabs.harvard.edu/abs/2015LPI....46.2452C (accessed November 27, 2015).

[61] O. Forni, M. Gaft, M.J. Toplis, S.M. Clegg, S. Maurice, R.C. Wiens, N. Mangold, O. Gasnault, V. Sautter, S. Le Mouélic, P.-Y. Meslin, M. Nachon, R.E. McInroy, A.M. Ollila, A. Cousin, J.C. Bridges, N.L. Lanza, M.D. Dyar, First detection of fluorine on Mars: Implications for Gale Crater's geochemistry, Geophys. Res. Lett. 42 (2015) 2014GL062742. doi:10.1002/2014GL062742.

[62] M. Nachon, N. Mangold, A. Cousin, R.B. Anderson, J.G. Blank, F. Calef, S. Clegg, C. Fabre, M. Fisk, O. Gasnault, L.C. Kah, R. Kronyak, J. Lasuer, P.-Y. Meslin, S. Le Mouélic, S. Maurice, D.Z. Oehler, V. Payre, W. Rapin, D. Sumner, K. Stack, S. Schröder, R.C. Wiens, Dagenetic Features Analyzed by ChemCam/Curiosity at Pahrump Hills, Gale Crater, Mars, in: 2015: p. 1524. http://adsabs.harvard.edu/abs/2015LPI....46.1524N (accessed November 27, 2015).

[63] D.W. Ming, P.D. Archer, D.P. Glavin, J.L. Eigenbrode, H.B. Franz, B. Sutter, M.S. Team, et al., Volatile and Organic Compositions of Sedimentary Rocks in Yellowknife Bay, Gale Crater, Mars, Science. 343 (2014) 1245267. doi:10.1126/science.1245267.

[64] M.L. Litvak, I.G. Mitrofanov, C. Hardgrove, K.M. Stack, A.B. Sanin, D. Lisov, W.V. Boynton, F. Fedosov, D. Golovin, K. Harshman, I. Jun, A.S. Kozyrev, R.O. Kuzmin, A. Malakhov, R. Milliken, M. Mischna, J. Moersch, M. Mokrousov, S. Nikiforov, R. Starr, C. Tate, V.I. Tret'yakov, A. Vostrukhin, Hydrogen and chlorine abundances in the Kimberley formation of Gale crater measured by the DAN instrument on board the Mars Science Laboratory Curiosity rover, J. Geophys. Res. Planets. 121 (2016) 2015JE004960. doi:10.1002/2015JE004960.

[65] M.L. Litvak, I.G. Mitrofanov, A.B. Sanin, D. Lisov, A. Behar, W.V. Boynton, L. Deflores, F. Fedosov, D. Golovin, C. Hardgrove, K. Harshman, I. Jun, A.S. Kozyrev, R.O. Kuzmin, A. Malakhov, R. Milliken, M. Mischna, J. Moersch, M. Mokrousov, S. Nikiforov, V.N. Shvetsov, K. Stack, R. Starr, C. Tate, V.I. Tret'yakov, A. Vostrukhin, the MSL Team, Local variations of bulk hydrogen and chlorine-equivalent neutron absorption content measured at the contact between the Sheepbed and Gillespie Lake units in Yellowknife Bay, Gale Crater, using the DAN instrument onboard Curiosity, J. Geophys. Res. Planets. 119 (2014) 2013JE004556. doi:10.1002/2013JE004556.

Samples	#	Type	Water content (wt. %)	Analysis	Reference materials at Gale crater
Basalt standards	10	Fragments	0.18 – 2.2	CHNS flash analyzer, FTIR	Igneous basaltic rocks [60]
Fluorhydroxyapatite and basalt mixtures	6	Pellets	0 – 0.84	Stoichiometry	Detection of apatites [61]
Hydroxyapatites and basalt mixtures	4	Pellets	0.85 – 1.69	Stoichiometry	
Opal fragments	12	Fragments	1.7 – 9.2	LOI, TGA	High-silica sediments [58]
Opal and basalt mixtures	5	Pellets	0 – 7.5	LOI, TGA, Stoichiometry	
Calcium sulfates	3	Pellets	0 – 20.9	TGA, Raman	Calcium sulfate veins [29]
Gypsum and basalt mixtures	5	Pellets	13.1 – 20.9	TGA	
Magnesium sulfates	2	Pellets	47.3-51.2	LOI	Magnesium sulfate concretions [62]

Table 1: Summary of all sample types used for the calibration and types of analysis performed (FTIR: Fourier transform infrared spectroscopy, LOI: loss on ignition, TGA: Thermogravimetric Analysis).

Parameter	Sample type	Range	H area	H normalized total	VNIR	cont	C658	C248	O778
Pressure	Bassanite pellet	7 - 17 mbar	22%	10%	10%	19%	9%	6%	6%
Distance	Mars dust (first shots)	2.2 - 4 m	48%	5%	6%	5%	25%	4%	1.7%
Laser energy	Mars dust (first shots)	10 - 14 mJ	24%	1.6%	1.0%	4%	19%	0.5%	3%
Focus	Bassanite pellet	± 34 steps	22%	15%	16%	13%	18%	13%	13%
shot-to-shot profile variations (water content > 2 wt.%)	Bassanite pellet	100 shots	21%	25%	28%	34%	22%	17%	16%
	Gypsum pellet	30 shots	23%	25%	27%	37%	8%	14%	16%
	Hexahydrite pellet	30 shots	13%	13%	15%	23%	3%	17%	5%
	Opal 1040 pellet	30 shots	7%	9%	10%	14%	9%	9%	6%
	Opal 1040 fragment	30 shots	30%	33%	37%	48%	24%	29%	26%
	Opal 1543a fragment	900 shots	42%	48%	57%	73%	42%	41%	37%
	Opal 1039 fragment	150 shots	22%	22%	26%	33%	16%	20%	18%
(water content < 2 wt.%)	Basalt standard	50 shots	11%	16%	15%	13%	13%	13%	11%
	Apatite pellet	50 shots	7%	7%	8%	9%	6%	8%	7%
	Basalt pellet	50 shots	21%	22%	23%	27%	21%	22%	22%

Table 2: Summary of the variations of the hydrogen signal observed when varying the experimental parameters in a given range in the laboratory, except for distance and laser energy which are tested using Mars data on dust. The amplitude of the variations is characterized by the relative standard deviation of the signal around the mean, for the hydrogen peak area (H area) and for each normalization type (total: total spectrum, VNIR: VNIR spectrum, cont: continuum, C 658: carbon doublet peak area at ~658 nm, C 248 carbon peak at 247.9 nm and O 778: oxygen peak triplet at ~778 nm). Color coding indicates higher (dark red) or lower (slight to no color) standard deviations for each row. For shot-to-shot profiles, shot-to-shot standard deviation is represented; for other parameters, point-to-point standard deviation.

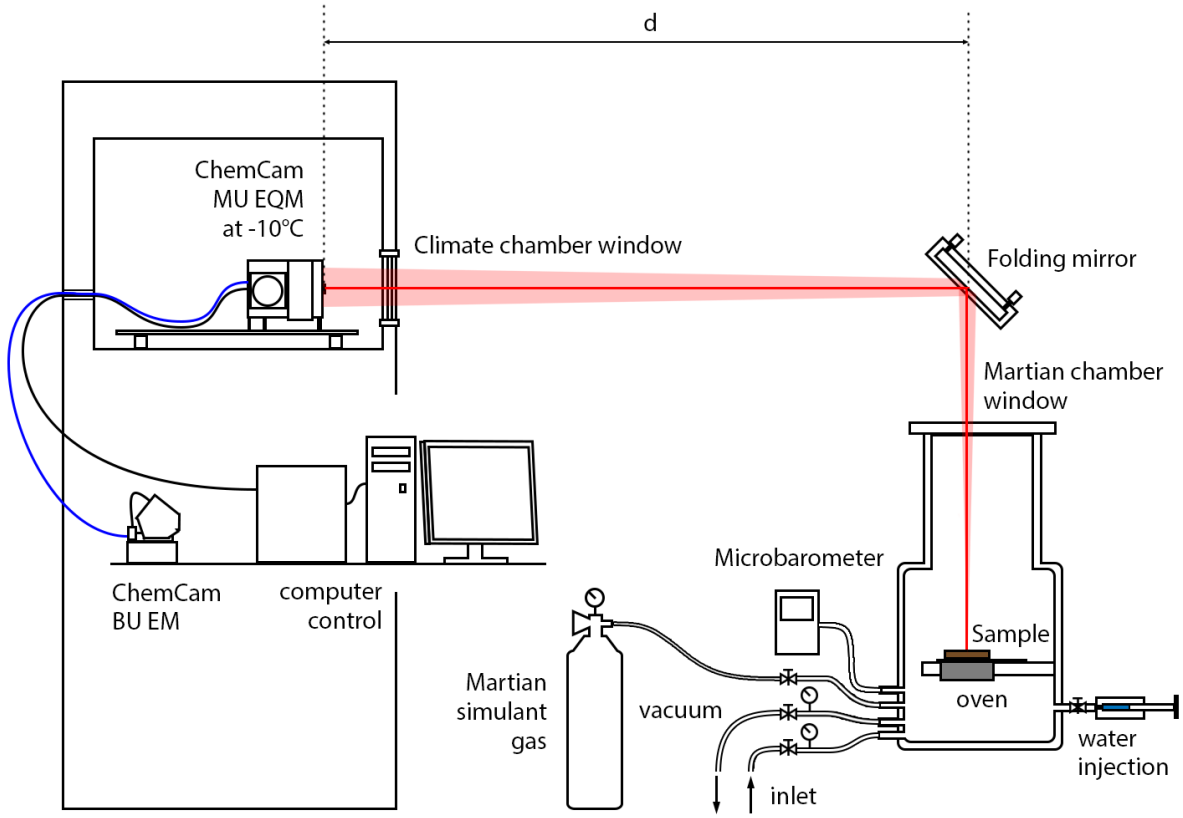

Figure 1: schematic of the ChemCam replica setup used for LIBS calibration in the laboratory.

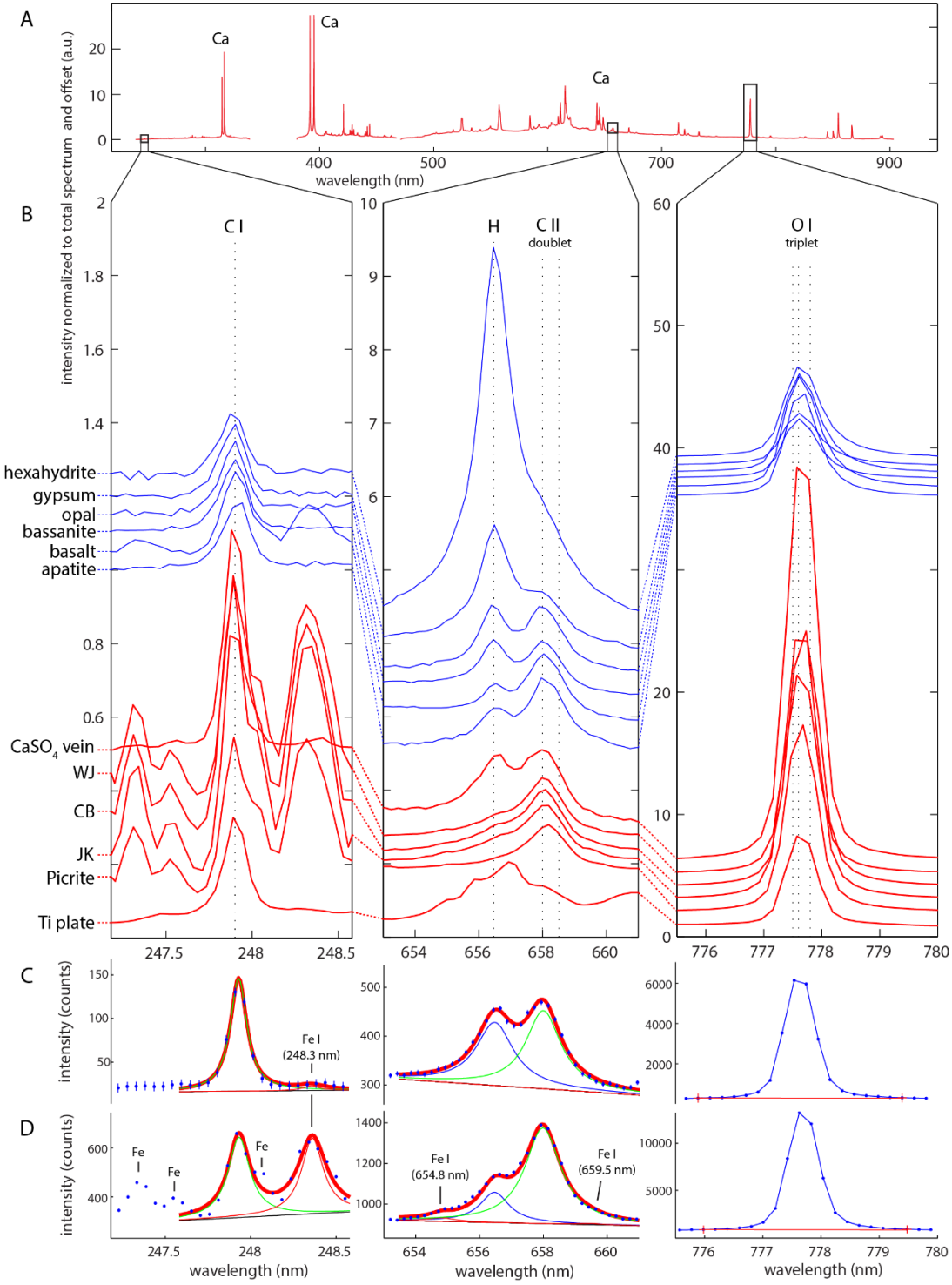

Figure 2: Example of ChemCam LIBS spectrum from apatite sample with spectral regions of interest (red boxes) (A). Close-up of spectral regions for different laboratory samples: hexahydrite, gypsum, opal, bassanite, basalt and apatite (blue), and examples of spectra acquired on Mars: a calcium sulfate vein, drill holes and calibration target picrate and titanium plate (red) (B). Spectra are normalized to the mean intensity and are offset for clarity. Data from drill holes are shown and named: WJ = Windjana, CB = Cumberland, JK = John Klein. The CaSO4 vein sample spectrum is taken from the target named 'Bird Spring' (sol 727). The 'picrite' is one of the ChemCam calibration targets onboard Curiosity [46]. On the bottom, peak fit of the apatite (C) and Windjana drill hole (D) spectra. The hydrogen (blue), carbon (green), iron (red) peak fits and the resulting total fits (thick red) are shown.

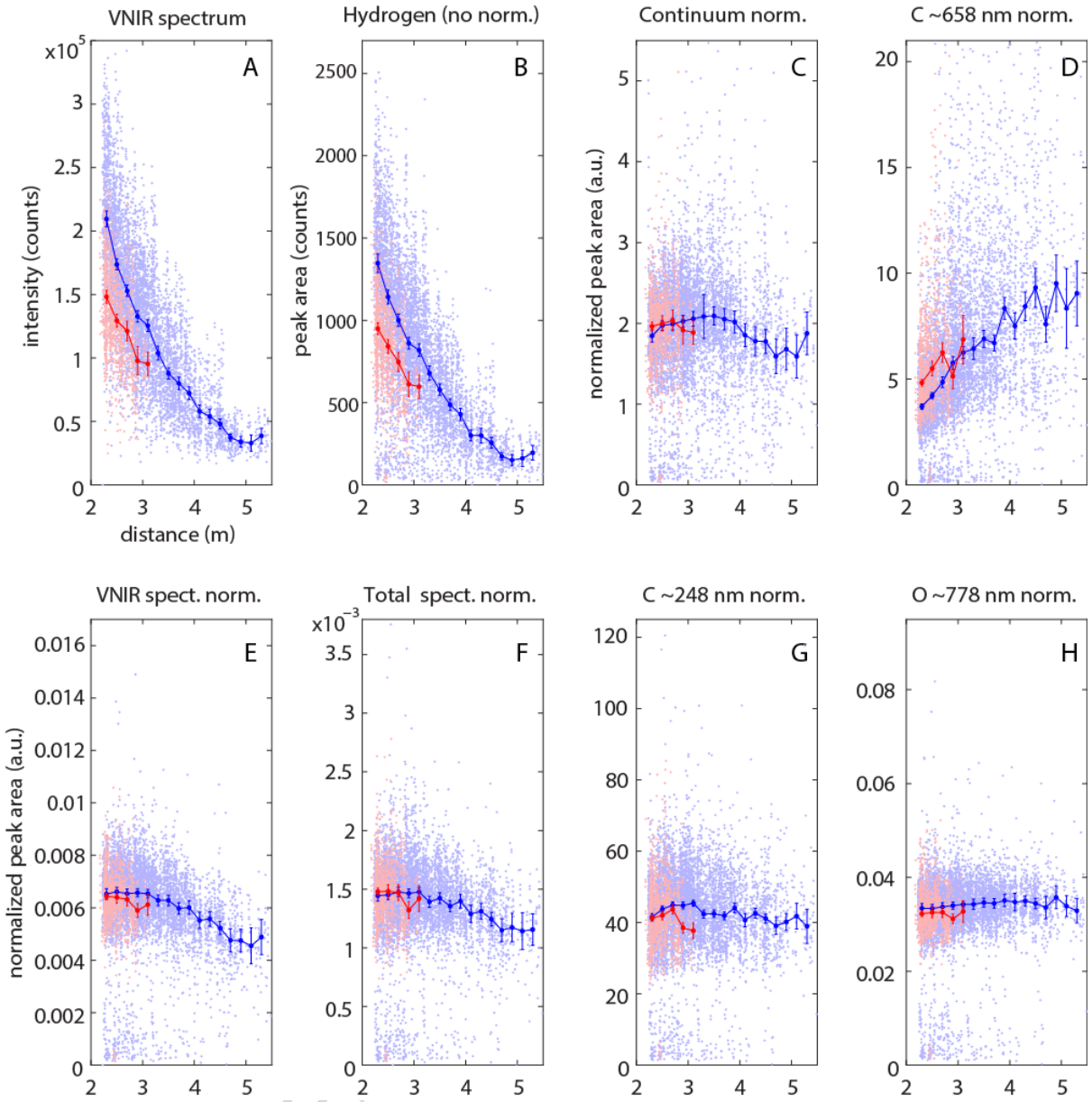

Figure 3: VNIR spectrum intensity (A) and hydrogen signal of the first shot for all ChemCam observations on Mars as a function of instrument distance to target (B). This hydrogen signal is shown after normalization to continuum emission (C), to the carbon peak at 658 nm (D), to the VNIR spectrum intensity (E), to the total spectrum intensity (F), to the neutral carbon peak at 248 nm (G) and oxygen peak (H). The data is shown for two laser energies used at Mars: ~14 mJ (blue) and ~10 mJ (red). Line with dots represents the average result for distance bins of 0.2 m. Error bars represent the 3-sigma uncertainty on the mean hydrogen signal within each distance bin (i.e. the standard deviation on the mean).

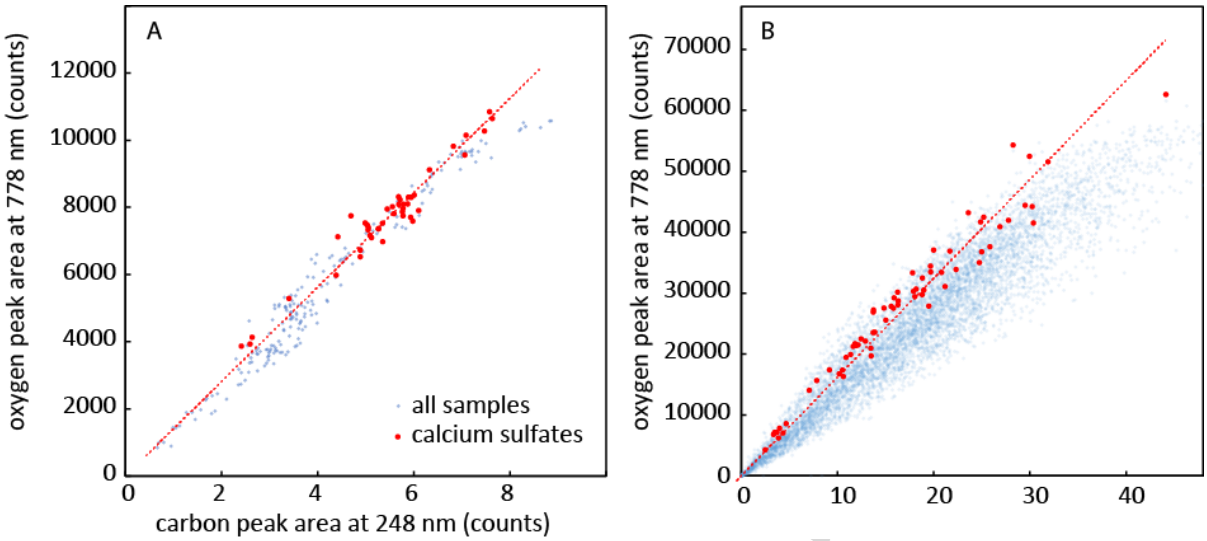

Figure 4: Oxygen peak area at 778 nm as a function of carbon peak area at 248 nm for LIBS data obtained in the laboratory (A) and on Mars (B). The data from calcium sulfates pellets (A red) and calcium sulfate veins analyzed on Mars (B red) is represented with corresponding linear regression (red dotted lines); along with data from all other samples (A blue) and from other targets analyzed on Mars up to sol 1248 (B blue). These figures show that the O/C ratio remains constant over a large range of experimental parameters, which enables us to derive the Mars/lab relative IRF between the 778 nm and 248 nm spectral regions from the ratio of the slopes.

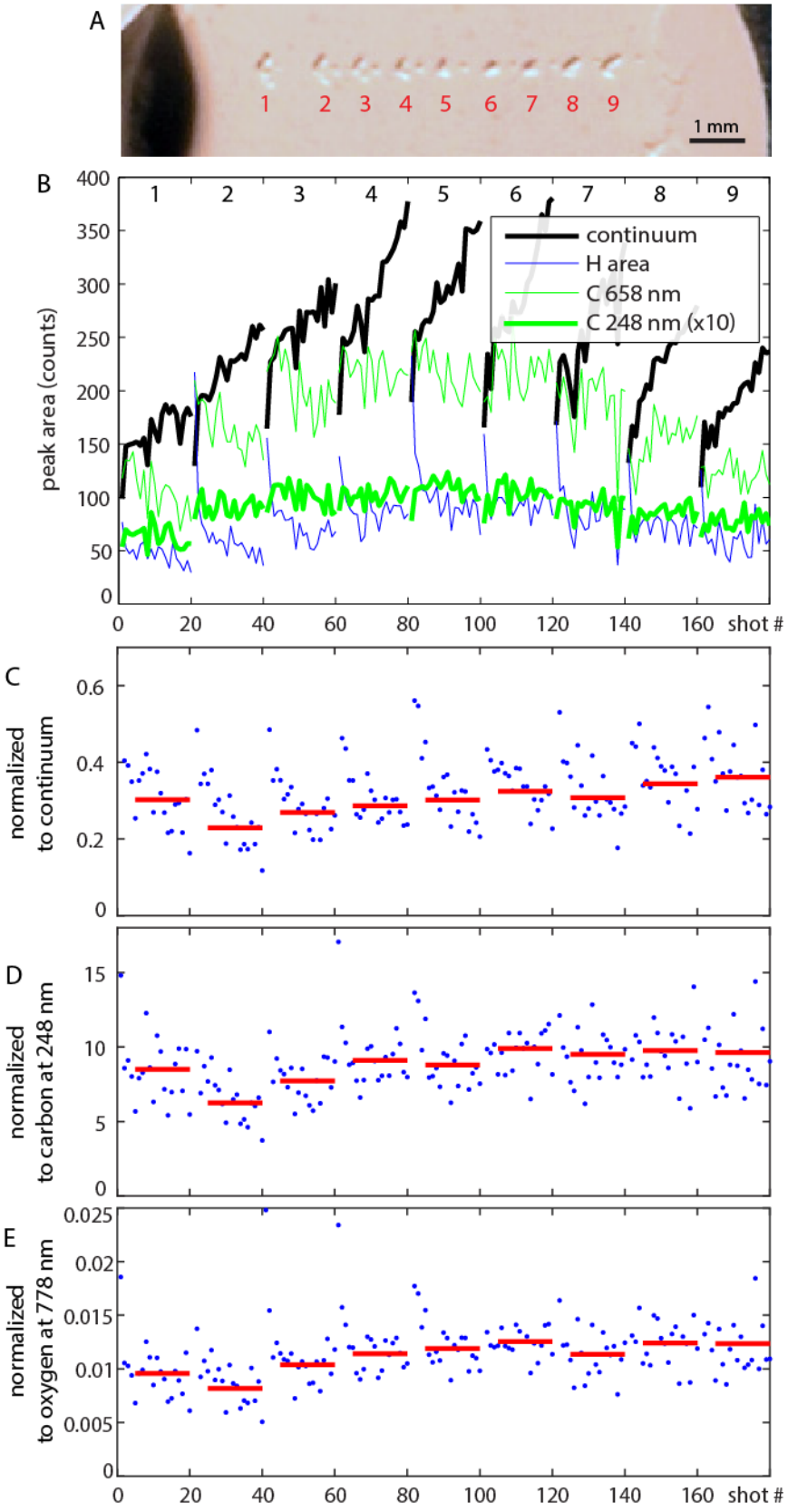

Figure 5: Peak area shot-to-shot series for hydrogen and carbon (B) when varying laser focus during tests on a bassanite pellet in the laboratory (A). The sequence represents 9 points of 20 shots each. The single shot hydrogen signal (blue dots) and point-to-point average without 5 first shots (red) are represented with normalization to continuum (C), carbon at 248 nm (D) and oxygen at 778 nm (E).

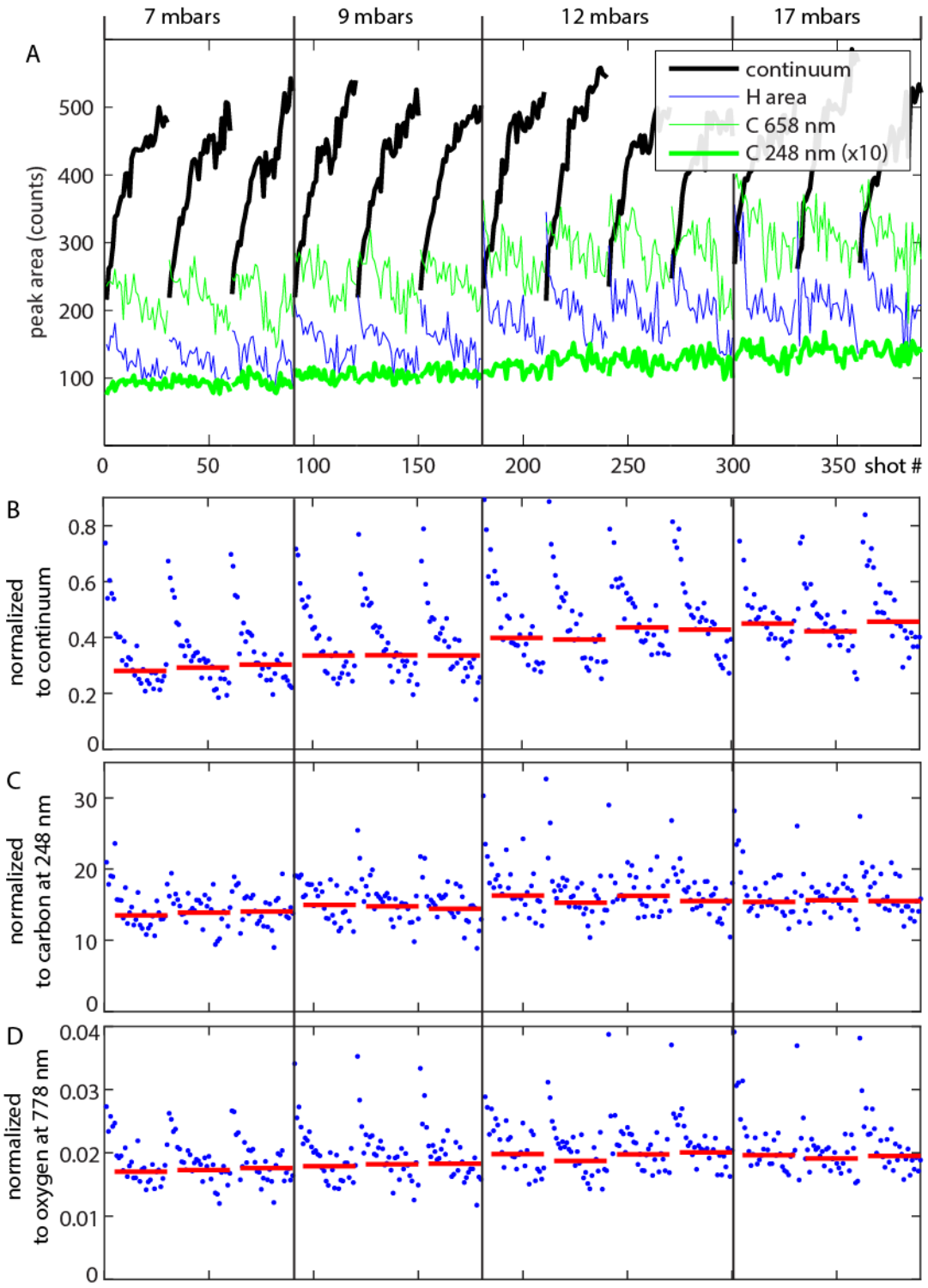

Figure 6: Peak area shot-to-shot series for hydrogen and carbon (A) when varying CO_2 pressure from 7 to 17 mbar during tests on a bassanite pellet in the laboratory. The sequence represents 13 points of 30 shots each. The single shot hydrogen signal (blue dots) and point-to-point average without 5 first shots (red) are represented with normalization to continuum (B), carbon at 248 nm (C) and oxygen at 778 nm (D).

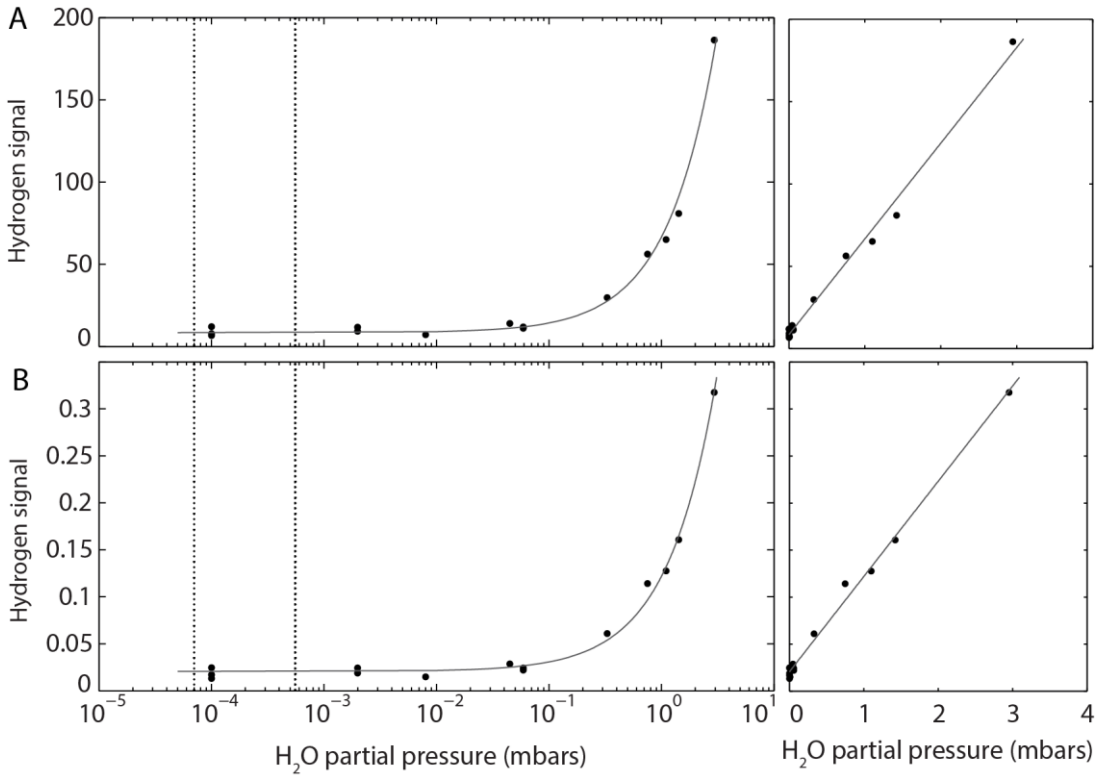

Figure 7: Hydrogen signal as a function of partial pressure of water added into the martian chamber atmosphere. A total pressure of 6.3 mbar was maintained, mixing water vapor with CO_2. The hydrogen peak area (black dots) is represented normalized to carbon peak area at ~248 nm (A) and oxygen peak area at ~778 nm (B) with linear regression (solid lines). Vertical dotted lines show the range of water vapor pressures measured at Gale crater by the REMS instrument (10 – 80 ppmv in mixing ratio) [51].

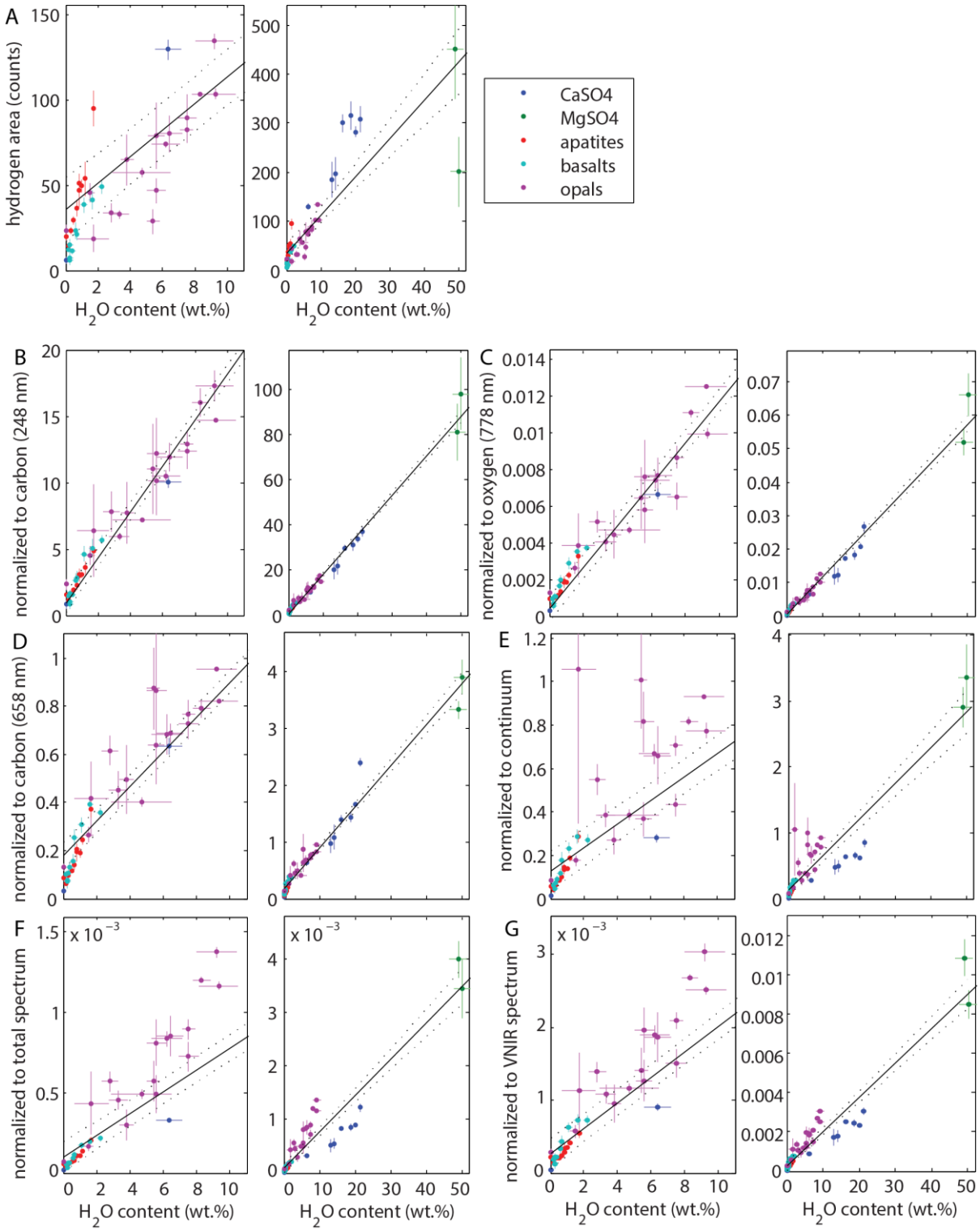

Figure 8: Calibration of the hydrogen signal with water content using different normalizations. For each calibration (A to G), left plot is a close-up of right plot. The vertical error bars correspond to the point-to-point standard deviation of the hydrogen signal for each sample, and the horizontal error bars correspond to the uncertainty on the samples water content, which depends on the technique used. The linear regression (black line) is represented for each normalization of the hydrogen signal along with the 95% confidence prediction interval (dotted lines).

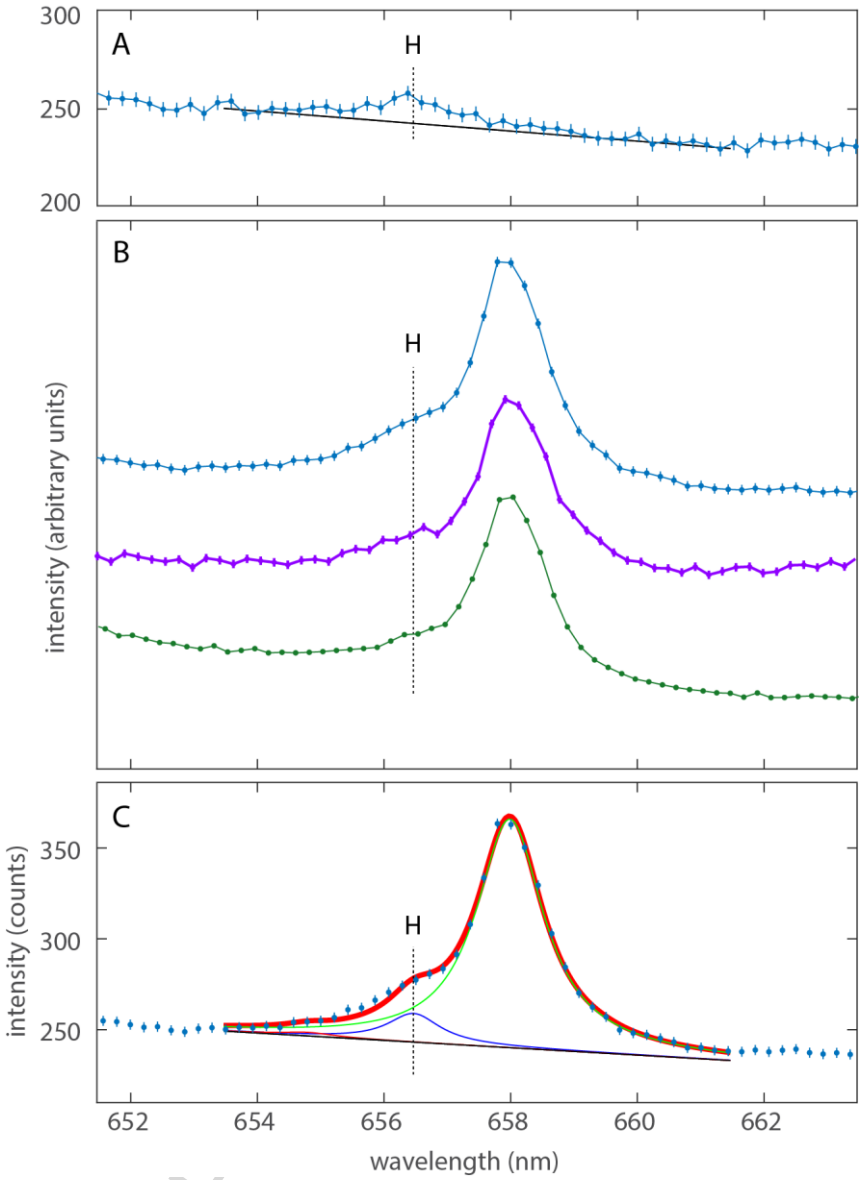

Figure 9: Close-up average spectrum obtained in the laboratory on a basalt sample containing 0.18 wt.% H_2O. The LIBS analyses have been performed under vacuum to check for the presence of a hydrogen signal without possible contribution from the atmospheric breakdown (A), and at martian pressure using CO_2 gas (B), with the corresponding fit (C). On plot (B), spectrum from the basalt sample (blue) is shown along with the silicon wafer (purple) and the anhydrite pellet (green). The linear baseline is represented as a solid black line (A and C), hydrogen and carbon peak fits in blue and green, respectively, and the total fit result in red (C).

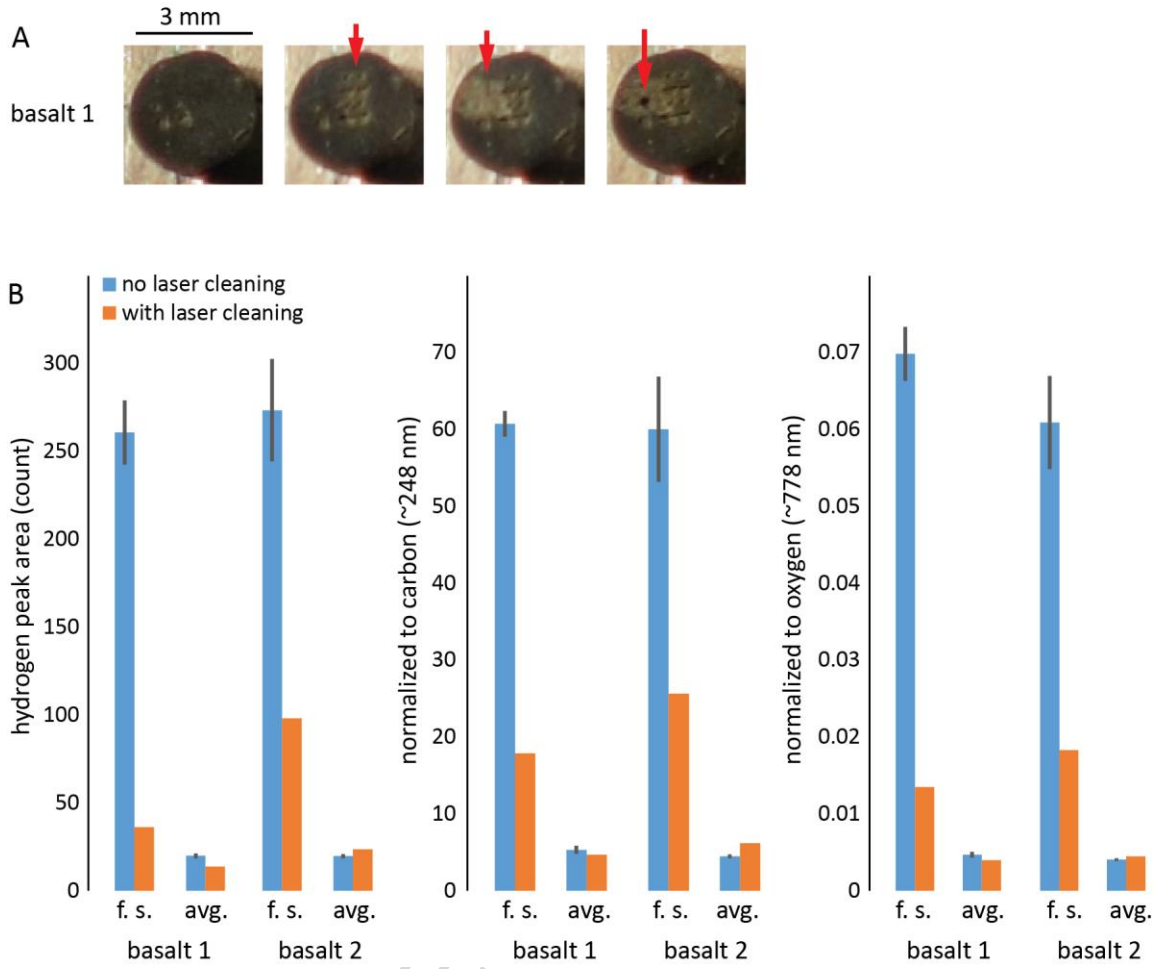

Figure 10: Results of the laser cleaning experiment on basalt standards (basalt 1: 0.18 wt.% H_2O, basalt 2: 0.12 wt.%). Close-up views (A) show the basalt sample surface; from left to right with red arrow indicating the change: sample before laser shots, group of laser pits before laser cleaning (50 shots per point), laser cleaning (resulted in lighter toned surface), 150 shot pit within laser cleaned surface. Hydrogen signal is represented (B) using no normalization and normalized to carbon and oxygen. For each sample, the hydrogen signal of the first shot (f.s.) spectra and of the average spectra without the 5 first shots (avg.) are represented.

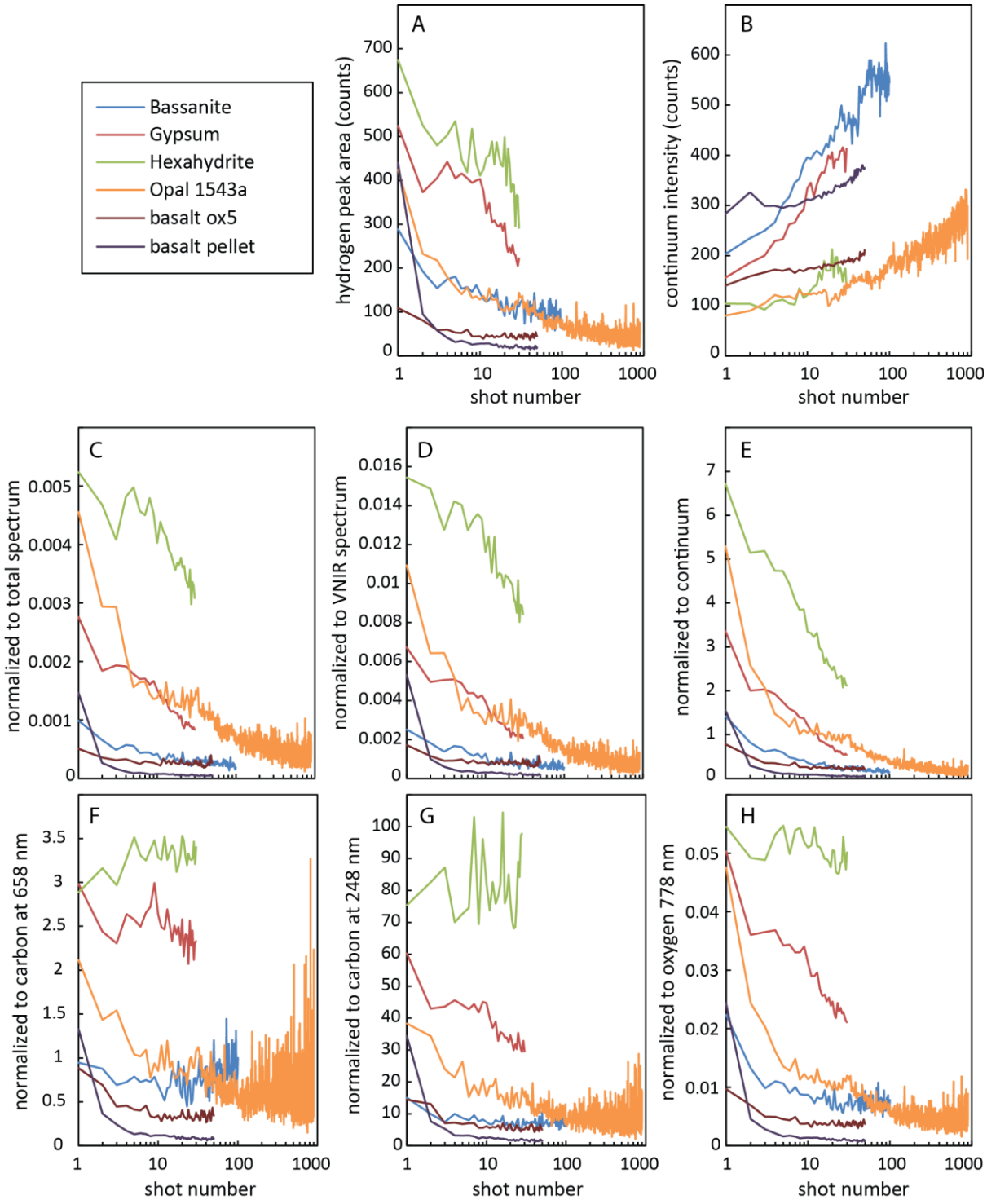

Figure 11: Shot-to-shot profiles of the hydrogen signal for several types of samples containing homogeneous water content and showing decrease of the hydrogen signal count (A). On the other hand, the continuum intensity shows continuous increase (B). Results using the different normalizations of the hydrogen signal are shown in plots C to H.

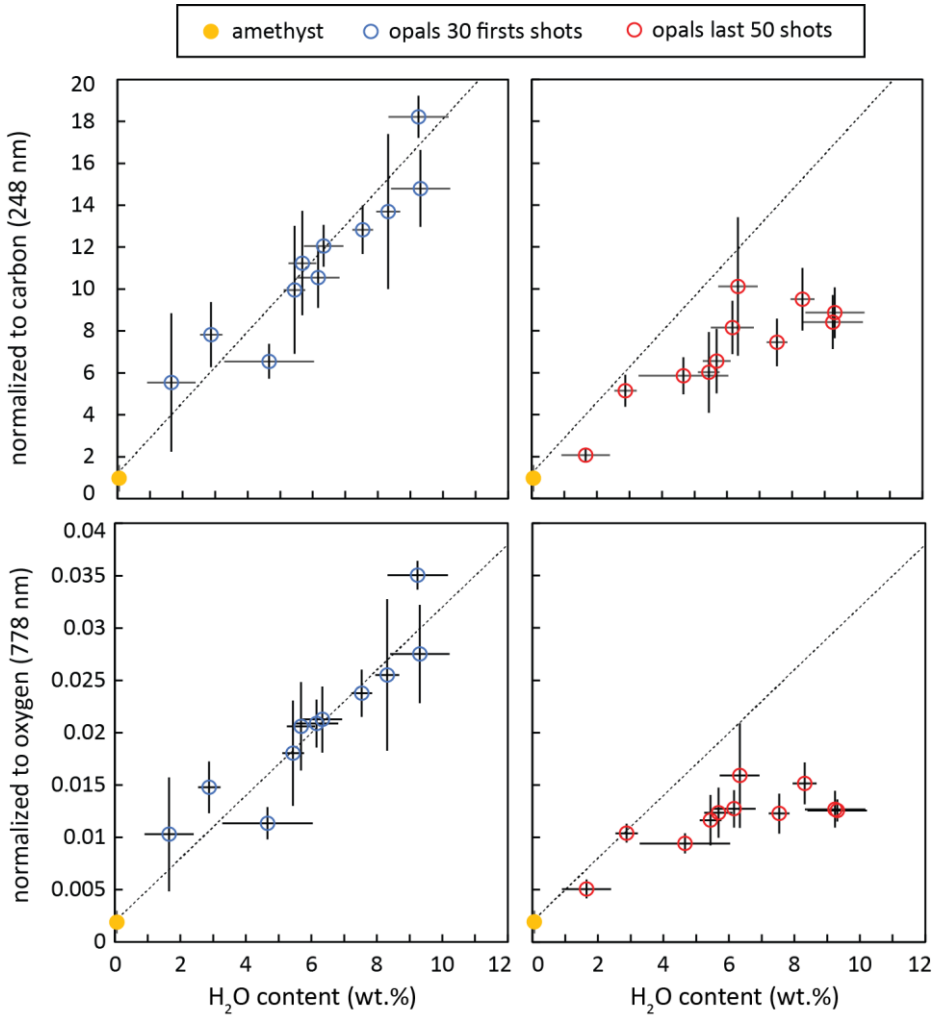

Figure 12: Hydrogen signal as a function of water content for different measurement protocols (i.e., number of shots/point). 150 shots profiles were performed on all opal samples. The hydrogen signal is represented as average of the shots 5 to 30 (blue circles) and as average of shots 100 to 150 (red circles). A natural amethyst sample, which contains only trace amounts of water, was analyzed similarly and data is shown (yellow circle) as a low hydrogen content reference. The calibration curve (dotted line) obtained for the first 30 shots data (all samples included) is also represented for reference (see fig. 8).

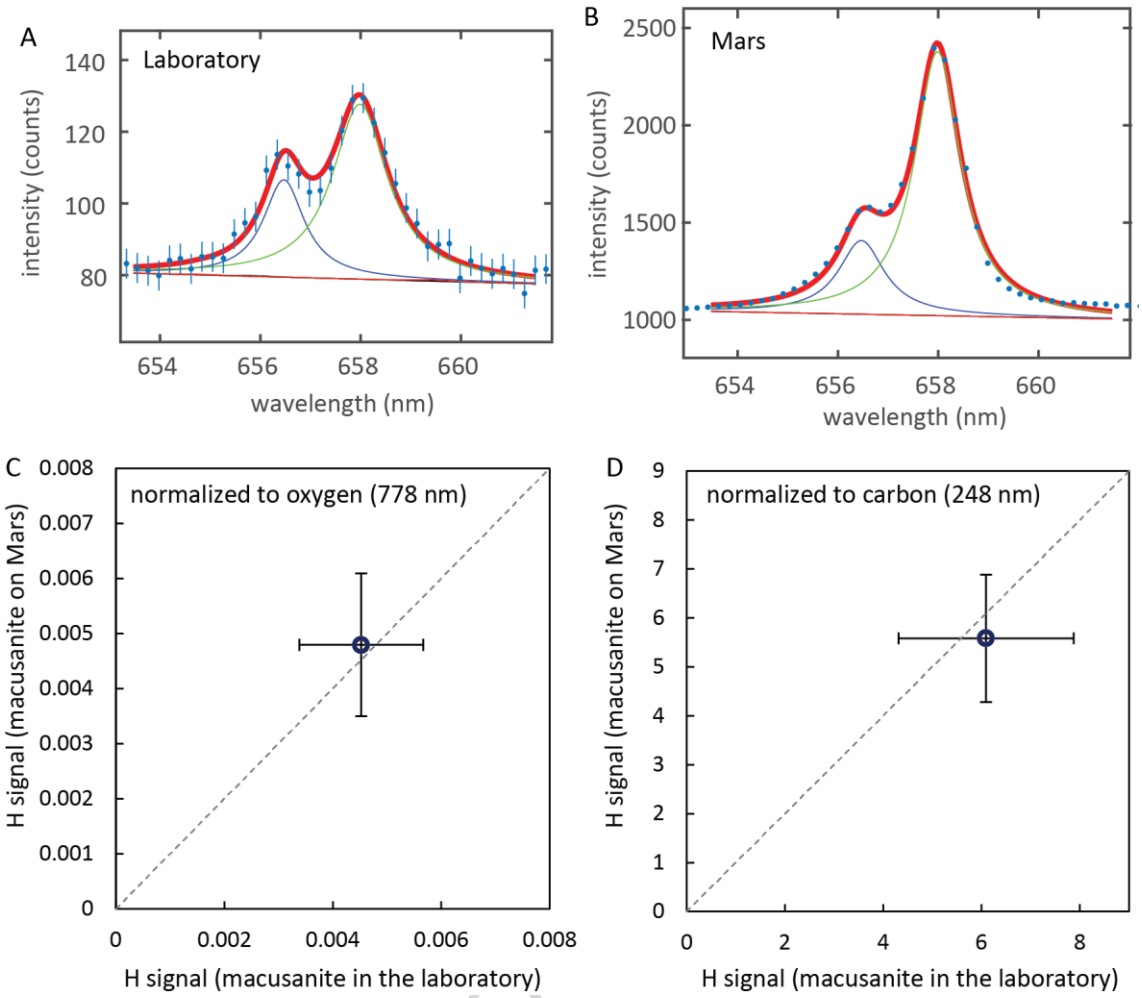

Figure 13: Fit result of the hydrogen signal (chart similar to figure 9-C) obtained on the macusanite calibration target in the laboratory (A) and on Mars (B). The corresponding Mars data is an average of 5 points taken with varying focalization around the best focus position on sol 862. In the laboratory the macusanite was set under vacuum for 24 hours, then 9 points were analyzed under 9.0 mbar of CO_2 with also varying focalization around the best focus position. The two signals normalized to the oxygen peak at 778 nm (C) or to carbon peak at 248 nm (D) match in both cases. The error bars represent 1-sigma uncertainties related to the point-to-point standard deviation and the IRF correction factor.

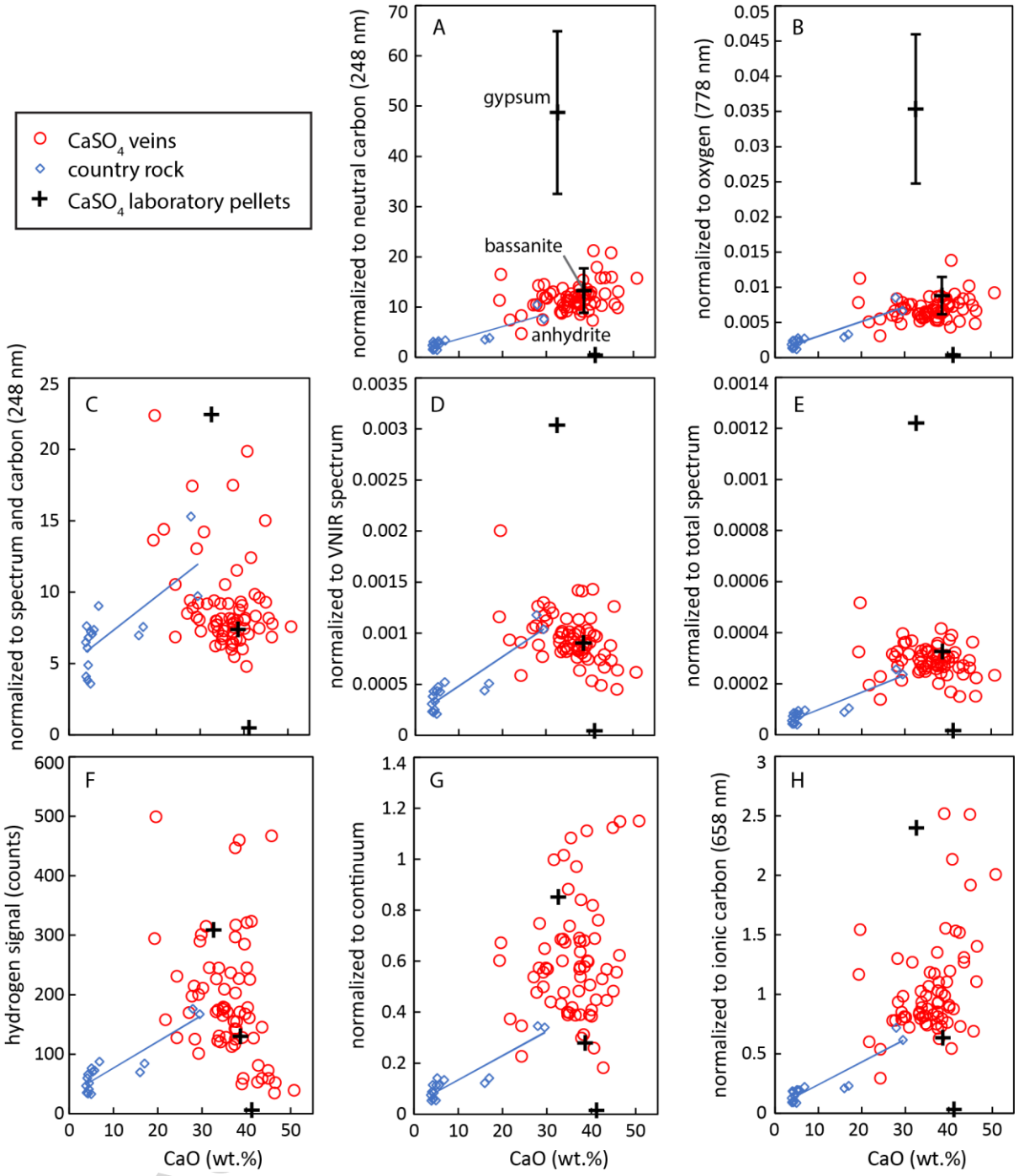

Figure 14: Hydrogen signal as a function of calcium oxide content using different normalizations, for veins analyzed on Mars (red circles) along with data from a drill hole country rock named "Telegraph Peak" including a veinlet (blue diamonds) with their linear regression (blue line); for more details on this dataset see Rapin et al. [41]. The hydrogen signal corresponding to laboratory pellets of calcium sulfates are represented as well (dark crosses). Plot F shows the hydrogen signal without normalization. On plots A and B, the error bars only represent the uncertainty on the true value related to IRF correction. The dispersion observed in martian data partly reflects variations of the experimental parameters as shown in table 2. Plot C shows data normalized to neutral carbon (248 nm) without IRF correction, but a normalization of the hydrogen area to the total VNIR spectrum and of the carbon area to the total UV spectrum has been applied.

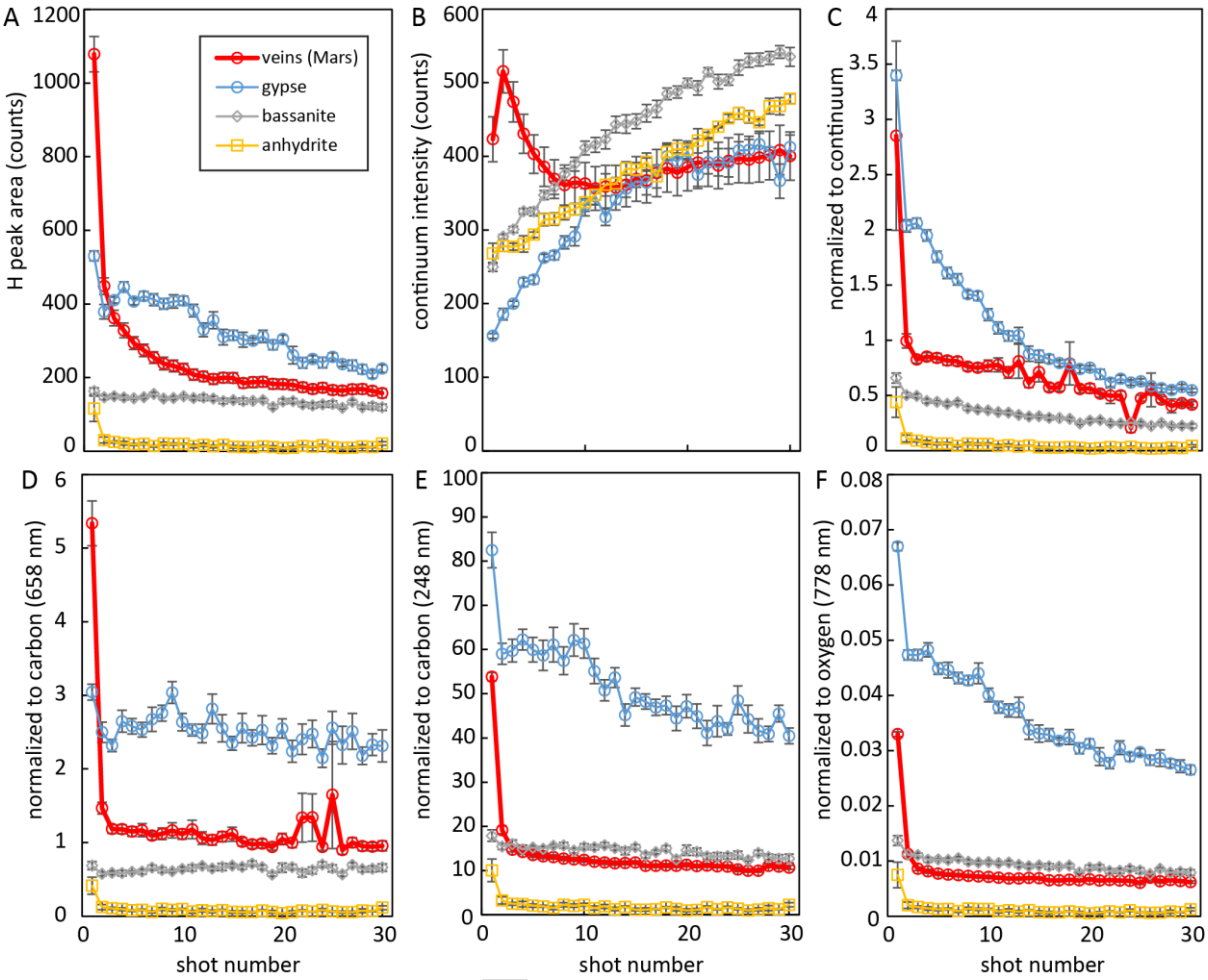

Figure 15: Shot-to-shot profiles of the hydrogen signal for calcium sulfates in laboratory and on Mars (red circles and lines) showing a decrease of the hydrogen signal (A). Conversely, the continuum intensity shows a continuous increase (B). Other normalizations of the hydrogen signal are represented in plots C to F. The vertical error bars represent the standard deviation for all shots performed at each shot number on the profile. Correction for IRF was applied for comparison to Mars for the normalization to carbon at 248 nm (E) and oxygen at 778 nm (F). However, the vertical error bars do not account for the uncertainty on the IRF correction (E and F).

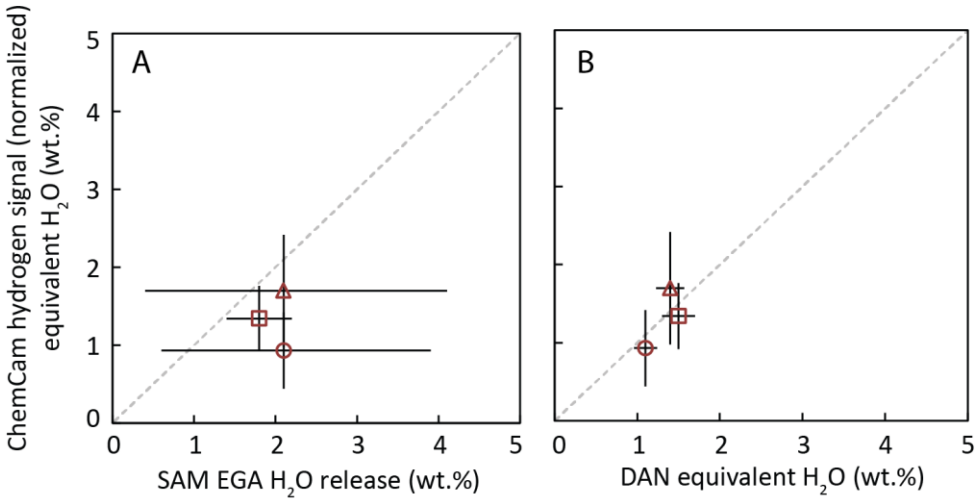

Figure 16: Water content obtained from ChemCam hydrogen signal on the drill samples against water content estimated by the SAM instrument evolved gas analysis [63,64] (A) and by the DAN measurements [64,65] (B) for the first 3 drill sites at Mars named: John Klein (circle), Cumberland (triangle), Windjana (square). The horizontal error bars represent the range of minimum to maximum values reported for the SAM EGA runs on the drill samples (A), and the reported DAN uncertainties (B) [64]. Vertical error bars include 1-sigma uncertainties related to the laboratory calibration and to the IRF correction factor.

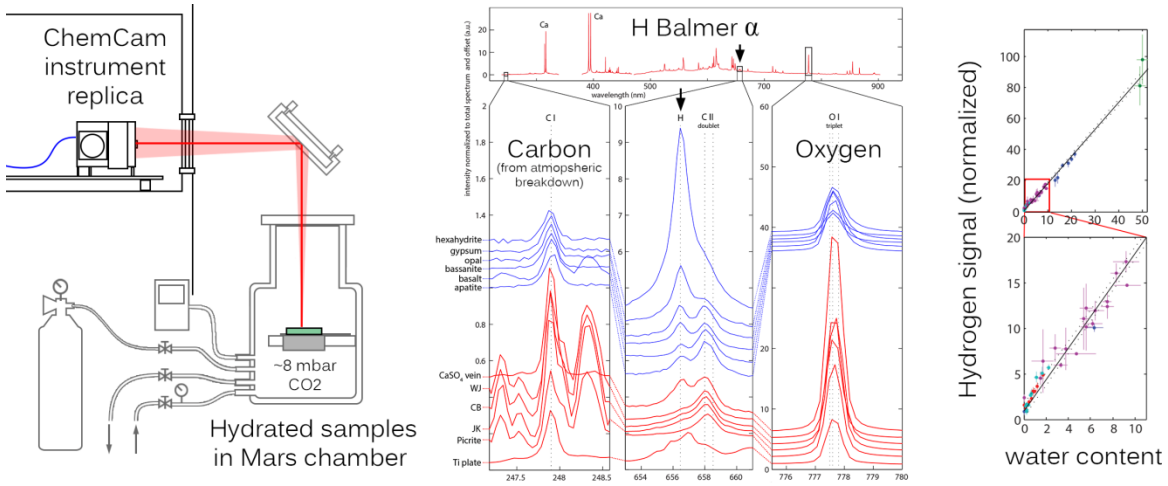

Graphical abstract